© 2018. Published by The Company of Biologists Ltd | Journal of Cell Science (2018) 131, jcs217992. doi:10.1242/jcs.217992

RESEARCH ARTICLE

Lipid bilayer stress-activated IRE-1 modulates autophagy during endoplasmic reticulum stress

Jhee Hong Koh*, Lei Wang*, Caroline Beaudoin-Chabot and Guillaume Thibault‡

ABSTRACT

Metabolic disorders, such as non-alcoholic fatty liver disease (NAFLD), are emerging as epidemics that affect the global population. One facet of these disorders is attributed to the disturbance of membrane lipid composition. Perturbation of endoplasmic reticulum (ER) homeostasis through alteration in membrane phospholipids activates the unfolded protein response (UPR) and causes dramatic transcriptional and translational changes in the cell. To restore cellular homeostasis, the three highly conserved UPR transducers ATF6, IRE1 (also known as ERN1 in mammals) and PERK (also known as EIF2AK3 in mammals) mediate adaptive responses upon ER stress. The homeostatic UPR cascade is well characterised under conditions of proteotoxic stress, but much less so under lipid bilayer stress-induced UPR. Here, we show that disrupted phosphatidylcholine (PC) synthesis in *Caenorhabditis elegans* causes lipid bilayer stress, lipid droplet accumulation and ER stress induction. Transcriptional profiling of PC-deficient worms revealed a unique subset of genes regulated in a UPR-dependent manner that is independent from proteotoxic stress. Among these, we show that autophagy is modulated through the conserved IRE-1–XBP-1 axis, strongly suggesting of the importance of autophagy in maintaining cellular homeostasis during the lipid bilayer stress-induced UPR.

KEY WORDS: Endoplasmic reticulum, ER, Unfolded protein response, UPR, Lipid bilayer stress, Autophagy, Metabolic disease

INTRODUCTION

Lipid content within cells is tightly regulated to maintain cellular homeostasis, and is crucial in many physiological processes including energy storage, signalling and membrane formation. The disruption in lipid homeostasis has been strongly associated with obesity and non-alcoholic fatty liver disease (NAFLD) (Puri et al., 2007; Tiniakos et al., 2010; Arendt et al., 2013; Doycheva et al., 2017), and is often characterised by excessive accumulation of lipids in liver, pancreatic and adipose tissues. Consequently, the inability of cells to alleviate such lipotoxic conditions results in a dysfunctional stress response and the induction of apoptosis, which, ultimately, leads to a disease state (Hotamisligil and Erbay, 2008; Rinella and Sanyal, 2015). Altered hepatic phospholipids levels have been observed in murine models of non-alcoholic hepatosteatosis (NASH), a more aggressive form of NAFLD, which can develop into hepatic fibrosis and hepatocellular carcinoma (HCC) (Li et al., 2006; Fu et al., 2011). Furthermore, the ratio of phosphatidylcholine (PC) to phosphatidylethanolamine (PE), the two major phospholipid species, has been associated with the survival and prognosis of liver function after partial hepatectomy in mice (Ling et al., 2012). As both PC and PE are the main lipids within the endoplasmic reticulum (ER) membrane, simultaneously blocking the two PC biosynthesis pathways, through ablation of the PE N-methyltransferase (*Pemt*) gene and the lack of dietary choline, leads to hepatic ER stress in mice, which correlates with steatosis progression (Li et al., 2005) (Fig. 1A). These observations link lipid bilayer stress (LBS), ER stress and metabolic disease progression.

The ER is the hub of protein folding for proteins targeted to the secretory pathway (Schroder and Kaufman, 2005; Braakman and Bulleid, 2011). In addition to its role in protein homeostasis, the ER is the site of lipid metabolism and provides majority of membrane lipids to the cell (Lagace and Ridgway, 2013; Wu et al., 2014). Long-term disruption of lipid homeostasis triggers chronic ER stress, which is associated with metabolic diseases (Fu et al., 2011; Han and Kaufman, 2016). To counter ER stress and maintain ER functionality, eukaryotes have evolved transcriptional and translational regulatory pathways collectively termed the unfolded protein response (UPR) (Cox and Walter, 1996; Schroder and Kaufman, 2005; Shen et al., 2004). The highly conserved UPR programme exerts homeostatic control by sensing accumulation of misfolded proteins or LBS at the ER (Walter and Ron, 2011; Volmer et al., 2013). As part of the programme, a subset of genes is upregulated to remodel various cellular pathways to ease stress and maintain viability, and the failure to reach ER homeostasis may result in cell death through apoptosis (Oyadomari et al., 2002; Wu et al., 2014; Mota et al., 2016).

In metazoa, the UPR consists of three conserved ER stress transmembrane transducers namely ATF6, IRE1 (also known as ERN1 in mammals) and PERK (also known as EIF2AK3 in mammals). Upon ER stress, each sensor activates their cognate downstream effectors resulting in general translational shutdown and the upregulation of target genes to restore cellular homeostasis (Walter and Ron, 2011; Wu et al., 2014). In the event of an acute response to excessive ER stress, the UPR programme leads to cell death through the IRE1 and PERK branches (Harding et al., 2003; Novoa et al., 2001). On the other hand, chronic ER stress triggers an adaptive response of the UPR programme that leads to differential expression of pro-survival signals and stabilisation of the UPR machinery, thereby bypassing apoptosis induction (Rutkowski et al., 2006; Rubio et al., 2011; Kim et al., 2017).

Previously, we have demonstrated that changes in membrane lipid composition through the ablation of the *de novo* PC biosynthesis gene *OPI3* (the *PEMT* orthologue) activate the essential intervention of the UPR to remodel the protein homeostasis network in budding yeast (Thibault et al., 2012;

School of Biological Sciences, Nanyang Technological University, Singapore 637551.
*These authors contributed equally to this work

‡Author for correspondence (thibault@ntu.edu.sg)

J.H.K., 0000-0002-4154-8369; L.W., 0000-0003-1729-874X; G.T., 0000-0002-7926-4812

Received 20 March 2018; Accepted 1 October 2018

Journal of Cell Science (2018) 131, jcs217992. doi:10.1242/jcs.217992

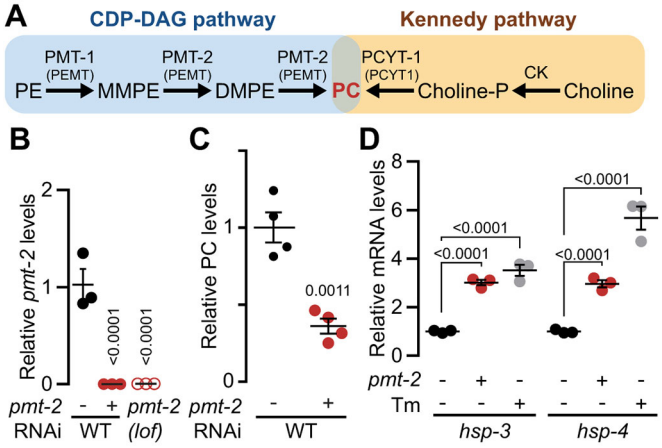

Fig. 1. *pmt-2* silencing is sufficient to activate the UPR by inducing LBS. (A) Metabolic pathways for the synthesis of phosphatidylcholine in *C. elegans*. Human orthologues are highlighted in brackets. PE, phosphatidylethanolamine; MMPE, monomethyl-phosphatidylethanolamine; DMPE, dimethyl-phosphatidylethanolamine; PMT-1/2, phosphatidylethanolamine N-methyltransferase 1/2; PEMT, phosphatidylethanolamine N-methyltransferase; PCYT-1, choline-phosphate cytidylyltransferase 1; CK, choline kinase. (B) qPCR results comparing expression of *pmt-2* in *pmt-2(RNAi)* and in *pmt-2(lof)* animals. (C) Comparison of relative PC levels in untreated WT and *pmt-2(RNAi)* animals as quantified by GC-FID. (D) qPCR results comparing the expression of UPR marker genes *hsp-3* and *hsp-4* in *pmt-2(RNAi)* and WT worms treated with 25 µg/ml Tm for 4 h. Data shown are the mean±s.e.m. of at least three independent experiments. *P*-values were calculated by one-way ANOVA followed by Tukey's multiple comparisons adjustment (B,D) or two-tailed Student's *t*-test (C).

Ng et al., 2017 preprint). The UPR is directly activated from ER membrane LBS independently from the accumulation of misfolded proteins (Promlek et al., 2011; Volmer et al., 2013; Ho et al., 2018; Tam et al., 2018). Similar to the NAFLD mouse model lacking the *Pemt* gene (Li et al., 2006, 2005) and our yeast model deleted for the *OPI3* gene (Thibault et al., 2012; Ng et al., 2017 preprint), *Caenorhabditis elegans* models have been developed to block PC synthesis via loss-of-function (herein denoted *lof*) mutations in the *PEMT* orthologues *pmt-1* and *pmt-2* or the upstream precursor S-adenosylmethionine synthetase *sams-1* (Brendza et al., 2007; Li et al., 2011; Walker et al., 2011; Ding et al., 2015) (Fig. 1A).

Excessive protein accumulation during proteotoxicity-induced ER stress has been shown to activate autophagy because the accumulation of misfolded proteins exceeds the capacity of the ER-associated degradation for their clearance (Kouroku et al., 2007; Senft and Ronai, 2015), but little is known on the role of autophagy during the LBS-induced UPR. In this study, we characterised the role of the UPR during chronic LBS-induced ER stress. We proposed that LBS may elicit a chronic ER stress response that is distinct from that resulting from acute ER stress. In *C. elegans*, we silenced *pmt-2* to attenuate PC synthesis in the UPR mutant animals *atf-6(lof)*, *ire-1(lof)* and *pek-1(lof)*. As expected, genetic ablation of *pmt-2* resulted in the perturbation of lipid homeostasis with significantly decreased PC levels, which then correlated with UPR activation. Although conventionally seen as a linear response to ER stress, our findings demonstrate a strikingly different outcome of the UPR programme when activated by LBS (hereafter denoted UPR^{LBS}) as opposed to proteotoxic stress (hereafter denoted UPR^{PT}). More importantly, we reveal that autophagy is modulated by the IRE-1–XBP-1 axis during the LBS-induced UPR, suggesting the importance of autophagy to maintain cellular homeostasis during LBS.

RESULTS

The attenuation of *pmt-2* activates the UPR by reducing total phosphatidylcholine

PMT-1 and *PMT-2* are both required for the synthesis of PC from PE in *C. elegans* (Palavalli et al., 2006; Brendza et al., 2007; Li et al., 2011) (Fig. 1A). In the absence of dietary choline, both genes are essential for the development of *C. elegans*, and silencing either gene from stage-one (L1) larvae onwards leads to sterility (Brendza et al., 2007). PC cannot be obtained from the standard laboratory worm diet as the conventionally used *E. coli* strains OP50 and HT115(DE3) lack PC (Morein et al., 1996; Oursel et al., 2007). Thus, PC levels in worms can be altered by genetically manipulating *pmt-1* or *pmt-2* to induce LBS thereby activating the UPR (Fig. S1C). To better understand the role of the UPR during LBS, we subjected synchronised L1 worms to *pmt-2* RNA interference (RNAi) for 48 h. Two-day RNAi feeding was sufficient to decrease *pmt-2* mRNA in wild-type (WT) animals to close to the background signal of *pmt-2(lof)* (Fig. 1B). As previously reported, *pmt-2*(RNAi) animals showed a developmental defect characterised by reduced body size, which could be rescued by choline supplementation (Fig. S1A,B) (Palavalli et al., 2006). PC is synthesised from choline through the Kennedy pathway (Fig. 1A). Supplementing *pmt-2(RNAi)* animals with 30 mM choline was sufficient to prevent UPR activation while the growth defect was alleviated with 60 mM choline (Fig. S1A–C). To further characterise *pmt-2(RNAi)* worms, PC was separated from the total lipid extract of worms by thin layer chromatography (TLC). This was followed by a transesterification reaction to derive fatty acid methyl esters (FAMEs) specifically from PC, which were further quantified via gas chromatography with a flame ionisation detector (GC-FID). We found that the PC level in *pmt-2(RNAi)* worms was markedly reduced to 36% of that in vector control worms (Fig. 1C). Attenuating *pmt-2* expression was not sufficient to fully eliminate PC in WT animals due to the large phospholipid reserve in stage L1 worms in addition to the long half-lives of phospholipids (Dowd et al., 2001). As LBS can lead to ER stress, we measured the transcriptional levels of the UPR-induced ER-resident molecular chaperone Hsp70 family (Urano et al., 2002). The mRNA levels for both of the *C. elegans* human Hsp70 family orthologues, *hsp-3* and *hsp-4*, were upregulated transcriptionally in *pmt-2(RNAi)* worms compared to WT (Fig. 1D). The mRNA level of *hsp-3* in *pmt-2(RNAi)* worms was similar to that of WT worms incubated with the strong UPR inducer tunicamycin (Tm) for 4 h. Tm inhibits protein *N*-glycosylation leading to a severe accumulation of unfolded proteins in the ER (Ericson et al., 1977). In contrast, the *hsp-4* mRNA level was remarkably higher in Tm-treated animals compared to those with LBS. This result suggests that *hsp-4* expression might be modulated differently by the UPR programme depending on the nature of the stress. As the UPR is activated by low PC, *C. elegans* subjected to *pmt-2* RNAi mimics NAFLD because altered PC:PE ratios and UPR activation are interconnected (Ozcan et al., 2004; Fu et al., 2011; Thibault et al., 2012; Ng et al., 2017 preprint).

Attenuated phosphatidylcholine synthesis leads to lipid droplet accumulation

To investigate the regulatory role of the three ER stress transducers during LBS (Shen et al., 2005), *atf-6(lof)*, *ire-1(lof)* and *pek-1(lof)* mutant worms were subjected to *pmt-2* RNAi as described above (Fig. S2A). The simultaneous ablation of two or three UPR branches is not possible as any combination is lethal (Shen et al., 2005). Treatment with *pmt-2* RNAi resulted in a reduction of PC

Journal of Cell Science (2018) 131, jcs217992. doi:10.1242/jcs.217992

across the three UPR mutants that was comparable to that seen in WT worms (Fig. 2A; Fig. S2B). The UPR transducers regulate lipid metabolism where XBP-1 downstream of IRE-1 is responsible for phospholipid synthesis (Sriburi et al., 2004). Hence, it is unsurprising that *ire-1(lof)* worms have decreased PC compared to WT in the untreated condition (Fig. 2A). To quantify the relative levels of the fatty acids (FAs) derived from PC and its precursor PE during LBS, both phospholipids were separated from total lipid extracts by TLC and quantified by GC-FID as described above. As expected, PC depletion in the UPR mutants and WT worms caused a significant reduction of all FAs derived from PC except for margaric acid (C17:0), α-linolenic acid (C18:3n3) and eicosadienoic acid (C20:2), indicating a general disturbance in the PC metabolic pathways during LBS (Fig. 2B). However, levels of FAs derived from PE were largely unmodified across the strains as *pmt-2* RNAi leads to the accumulation of the downstream phospholipid intermediate monomethyl-phosphatidylethanolamine (MMPE) (Fig. 1A). As a reduction in PC level leads to lipid droplet (LD) accumulation in eukaryotes (Li et al., 2011; Walker et al., 2011; Thibault et al., 2012; Hörl et al., 2011), Sudan Black staining of fixed worms treated with *pmt-2* RNAi was carried out to visualise lipid droplets by Nomarski microscopy (Fig. 2C; Fig. S3A). To compare LD expansion in *pmt-2* RNAi-treated worms, the diameter of LDs was measured and classified into small (0.8–3 µm), medium (3.1–6 µm) and large (>6 µm) groups. We observed accumulation of large LDs but fewer total LDs in WT, *atf-6(lof)*, *ire-1(lof)*, and *pek-1(lof)* worms treated with *pmt-2* RNAi, corresponding to previous study in *sams-1(lof)* worms, where PC is also reduced (Ding et al., 2015).

To ensure that *pmt-2* RNAi treatment is sufficient to induce ER stress in the UPR mutants, we monitored the mRNA expression of two downstream target genes of IRE-1, *hsp-3* and *hsp-4*, by quantitative RT-PCR (qPCR). As expected, the levels of both the ER-resident chaperones *hsp-3* and *hsp-4* levels were significantly increased upon *pmt-2* RNAi and Tm treatments in WT and mutant strains with the exception of *ire-1(lof)* (Fig. 2D,E). Activation of the UPR from LBS was further validated *in vivo* by immunoblotting using the *phsp-4::gfp* reporter animal (Calfon et al., 2002). Consistent with the increase in *hsp-4* mRNA levels, *pmt-2* RNAi treatment resulted in an almost 2-fold increase in GFP in *phsp-4::*

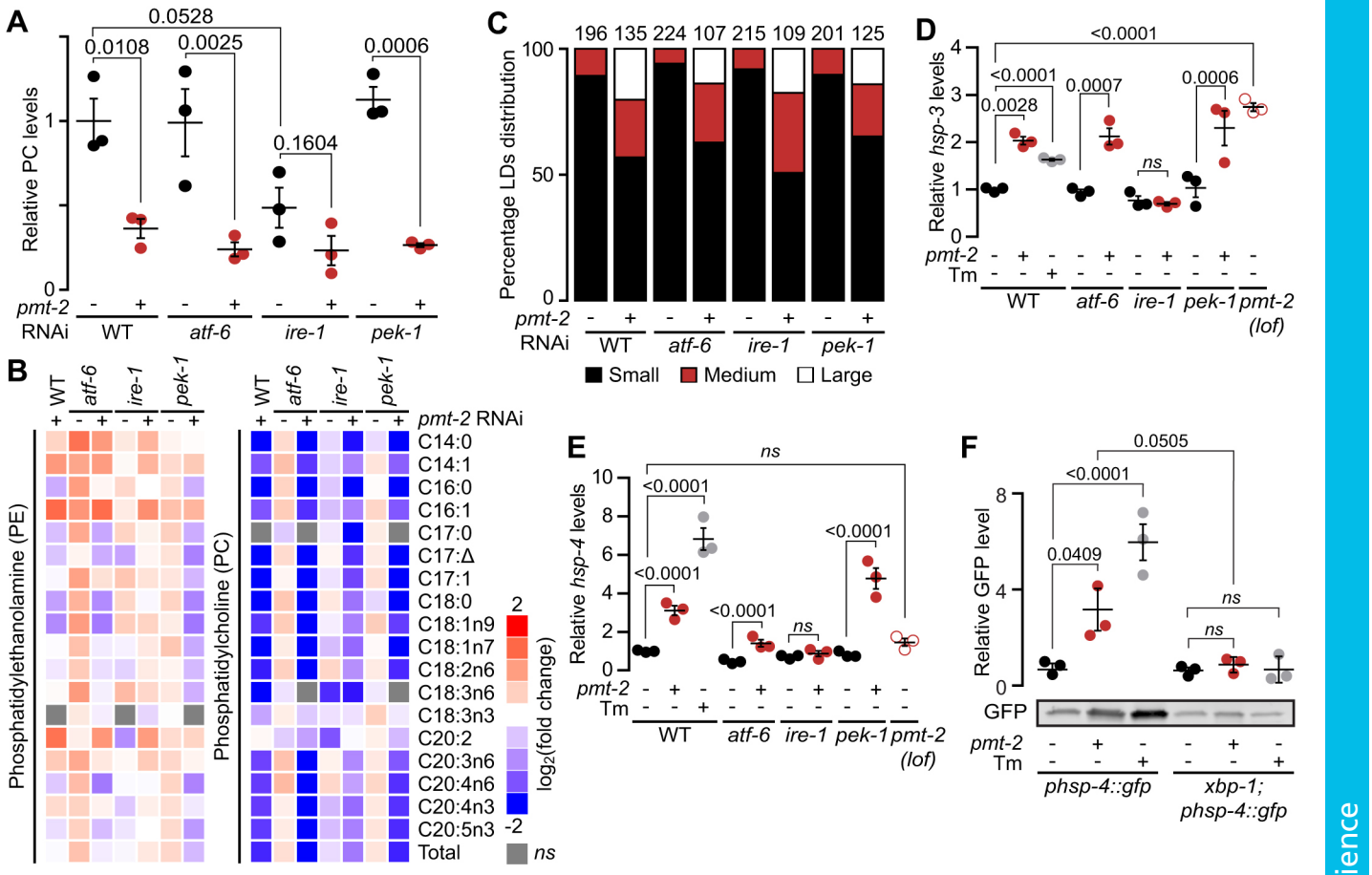

Fig. 2. UPR^{LBS} leads to the accumulation of lipid droplets. (A) Comparison of PC levels in WT, *atf-6(lof)*, *ire-1(lof)* and *pek-1(lof)* animals treated with *pmt-2* RNAi as quantified by GC-FID relative to that in untreated WT. (B) Heat map representation of all significant PE- and PC-derived FA changes relative to untreated WT. WT and mutant worms were treated as in A. (C) Lipid droplet (LD) size distribution quantified from bright-field images of Sudan Black B staining of WT and mutant animals treated as in A. LD sizes are classified into small (0.8–3 µm), medium (3.1–6 µm) and large (>6 µm) categories. Numbers above each bar refer to the mean number of lipid droplets present per worm. WT, n=12 (–), n=15 (+); *atf-6(lof)*, n=13 (–), n=14 (+); *ire-1(lof)*, n=18 (–), n=14 (+); *pek-1(lof)*, n=12 (–), n=13 (+), respectively. Representative images are shown in Fig. S3A. (D,E) qPCR results comparing the expression of UPR marker genes *hsp-3* and *hsp-4* in WT and mutant animals treated as in A and WT worms treated 4 h with 25 µg/ml Tm. (F) Quantification of anti-GFP antibody immunoblot signalling of worms treated as in A, with results normalised to values obtained with REVERT Total Protein Stain (a representative blot is shown in Fig. S3B). Data shown are the mean±s.e.m. of at least three independent experiments. *P*-values were calculated by one-way ANOVA followed by Tukey's multiple comparisons adjustment. ns, not significant.

Journal of Cell Science (2018) 131, jcs217992. doi:10.1242/jcs.217992

gfp animals, while Tm induced stronger upregulation (Fig. 2F). As expected, an increase in GFP was not detected in *xbp-1;phsp-4::gfp* animals treated with *pmt-2* RNAi nor with Tm, as HSP-4 is specifically upregulated from the IRE-1–XBP-1 axis upon ER stress (Acosta-Alvear et al., 2007).

UPR^{LBS} upregulates a different subset of genes from UPR^{PT}

Several studies suggest that the essential role of the UPR in maintaining metabolic and lipid homeostasis is highly conserved across species (for reviews, see Volmer and Ron, 2015; Han and Kaufman, 2016). A novel ER stress-sensing mechanism has been proposed in which the UPR is activated by lipid bilayer stress independently of unfolded protein accumulation in the ER (Promlek et al., 2011; Volmer et al., 2013; Halbleib et al., 2017). Thus, ER stress triggered by proteotoxic stress or LBS might differentially modulate the UPR to reach cellular homeostasis. To address whether this occurs, DNA microarray analysis was performed using RNA extracted from WT, *atf-6(lof)*, *ire-1(lof)* and *pek-1(lof)* animals treated with *pmt-2* RNAi. WT worms incubated with Tm for 4 h were included in the analysis to identify genes modulated by UPR^{PT} and subsequently uncouple those specifically modulated by UPR^{LBS}. To validate the quality of microarray data, qPCR was performed on a subset of genes (Fig. S4A,C). Overall, 2603 and 1745 genes were upregulated and downregulated, respectively, in *pmt-2(RNAi)* animals compared to WT (Fig. 3A, Table S2, data deposited in the Gene Expression Omnibus database under code GSE99763). In addition, Tm-treated WT worms showed upregulation of 1258 genes and downregulation of 1473 others. Only 492 and 420 genes were similarly upregulated and downregulated, respectively, from both UPR^{LBS} and UPR^{PT}, thereby suggesting these groups of genes are commonly modulated from the UPR regardless of the source of ER stress.

To explore how the UPR elicits a differential stress response during LBS and proteotoxic stress, we filtered the 2111 gene candidates that were upregulated only in *pmt-2(RNAi)* animals and excluding genes upregulated in Tm-treated animals, respectively. Genes with unaltered expression in at least one of the UPR mutants subjected to *pmt-2* RNAi are considered to be modulated by UPR^{LBS}. From these criteria, 1069 genes were upregulated in a UPR^{LBS}-dependent manner (Fig. 3B; Table S3). We identified 181, 417 and 25 genes that are specifically upregulated from the ATF-6, IRE-1 and PEK-1 branches of the UPR, respectively, while 446 genes were modulated from at least two of the three UPR branches, suggesting compensatory roles of one or more UPR transducers in the absence of the other branches. In addition, we grouped genes with at least a 1.5-fold change in expression level by hierarchical clustering (Fig. 3C; Table S4). This allowed us to visualise genes that were similarly regulated throughout the array from UPR^{LBS}. Manual inspection of our array data demonstrates that the upregulation of known UPR target genes are in agreement with previous reports (Fig. 3D) (Travers et al., 2000; Shen et al., 2005; Thibault et al., 2011).

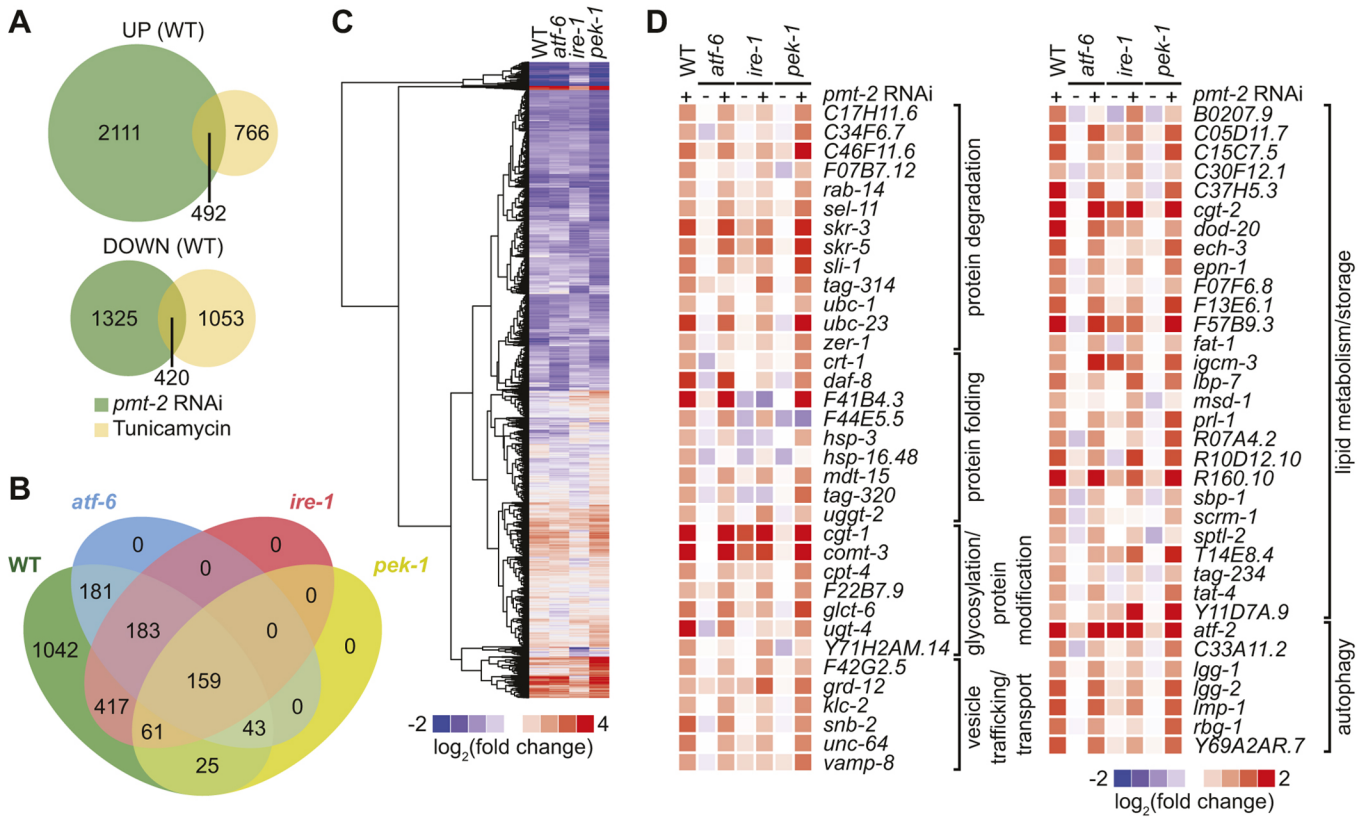

Fig. 3. UPR^{LBS} and UPR^{PT} lead to distinct transcriptomic outcomes. (A) Venn diagram representation of upregulated (UP) and downregulated (DOWN) genes at a minimum of 1.5-fold in *pmt-2(RNAi)* and WT worms treated with 25 µg/ml Tm for 4 h compared to untreated WT worms. (B) Four-way Venn diagram depicting transcriptional targets of WT, *atf-6(lof)*, *ire-1(lof)* and *pek-1(lof)* worms that are upregulated during LBS and excluding genes commonly upregulated after *pmt-2* RNAi and Tm treatments. Shown are number of genes giving fold changes that were >1.5 and at $P<0.05$ (ANOVA). (C) Hierarchical clustering of 8045 genes with significant changes based on Pearson correlation coefficients. Gene expression of WT, *atf-6(lof)*, *ire-1(lof)*, *pek-1(lof)* worms treated with *pmt-2* RNAi were compared against their respective untreated worms (empty vector). (D) Heat maps of selected *C. elegans* UPR-regulated genes previously listed by Travers et al. (2000). Based on $\log_2$ fold changes in gene expression normalised to untreated WT worms.

Journal of Cell Science (2018) 131, jcs217992. doi:10.1242/jcs.217992

To further understand the role of the UPR^{LBS} programme, we performed functional annotation for the 1069, 181, 417 and 25 upregulated genes identified from *pmt-2(RNAi)*, *atf-6(lof)*; *pmt-2(RNAi)*, *ire-1(lof)*; *pmt-2(RNAi)*, and *pek-1(lof)*; *pmt-2(RNAi)* animals, respectively, using the gene ontology (GO) tool DAVID (Table S5) (Huang et al., 2007). Immune regulatory genes were found to be enriched in the upregulated categories of WT and *ire-1* animals (Fig. 4A,C). This is in agreement with a previous report where innate immunity was found to be modulated by *sams-1*, the methyl donor to *pmt-1* and *pmt-2* (Ding et al., 2015). Our data suggest that innate immune response is positively and negatively regulated by IRE-1 and PEK-1, respectively (Fig. 4C,D). As expected, GO terms related to ER stress were found to be enriched in the upregulated categories of WT and mutant animals when PC is depleted (Fig. 4A–D) (Ding et al., 2015). We also identified an enrichment of downregulated genes in WT related to translational initiation factors including *eif-1.A*, *eif-3.C* and *eif-3.E*, a characteristic effect of UPR activation (Ling et al., 2009; Long et al., 2002).

Protein tyrosine phosphatase activity is significantly regulated by ATF-6 upon LBS (GO ID 0035335, n=6, Benjamini P-value of 0.047) (Fig. 4B). This class of genes is activated in response to ER stress (Agouni et al., 2011). Transcriptional regulation (GO ID 0006355, n=49, Benjamini P-value of 3.3×10^{-9}) is enriched among IRE-1-dependent genes and supports the evidence that they alleviate ER stress through a widespread transcriptional modification process (Fig. 4C) (Ng et al., 2000). In addition, genes involved in lipid and fatty acid processes were also enriched by IRE-1 and PEK-1 (Fig. 4C,D). Finally, protein tyrosine phosphatase activity (GO ID 0004725, n=4, Benjamini P-value of 0.039) is enriched by PEK-1, suggesting its involvement in protein modifications and the cell signalling cascade during LBS (Fig. 4D) (Bettaieb et al., 2012). Interestingly, we observed upregulation of autophagy-related processes that are IRE-1-dependent, as shown in the volcano plot [where autophagy-related genes with at least a 1.5-fold change and false discovery rate (FDR) P<0.05 were displayed on the plot; Fig. 4C,E]. Crosstalk between the UPR and autophagy in the context of protein clearance has been well documented (for a review, see Mizushima and Komatsu, 2011).

The IRE-1–XBP-1 axis regulates autophagy during UPR^{LBS}

To investigate whether the autophagic process is activated during the UPR^{LBS}, we carried out an RNAi screen of autophagy-related genes. To decrease PC levels, WT worms were first subjected to 36 h of *pmt-2* RNAi followed by 5 days of autophagy-related gene RNAi treatment (Fig. 5A). Phenotypes following RNAi treatment were classified as 0 (little difference in growth and brood size), 1 (smaller brood size, sick), and 2 (sterile, very sick) compared to vector control. The screen was carried out twice, and scores were designated for both WT animals pre-treated with vector and *pmt-2* RNAi. An RNAi candidate was classified as a positive hit if the sum of the scores in our phenotype scoring was equal to or exceeded 3 (Table S6). From the 40 RNAi clones, seven were found to induce development defects upon RNAi treatment compared to vector control (Fig. S5). As positive controls, we incorporated *ero-1* and *pmt-2* RNAis, as either lead to developmental defects and sterility (Rual et al., 2004; Palavalli et al., 2006). The screen revealed that some autophagy-related genes are required during UPR^{LBS} and their absence contributes to the observed detrimental phenotypes. Identified genes include *atg-7* (the orthologue of human ATG7, involved in autophagosome conjugation), *atg-13* (the orthologue of human ATG13, involved in autophagosome formation), *bec-1* (the

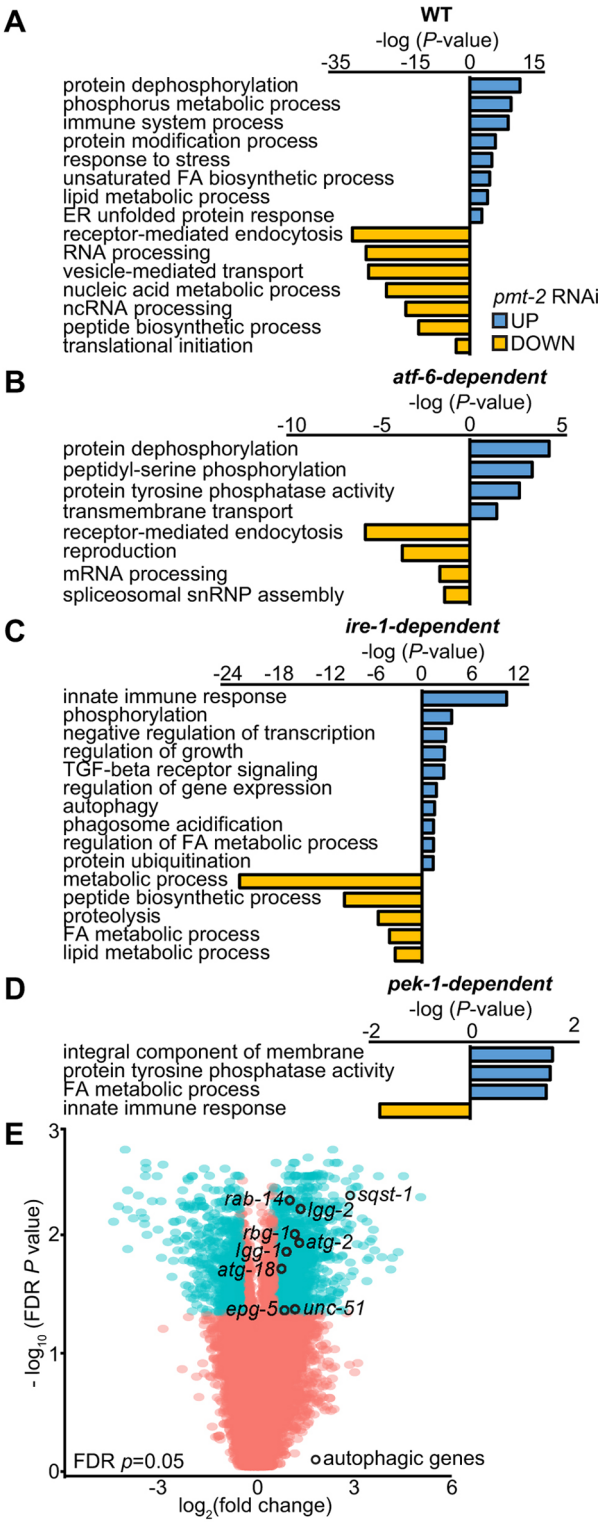

Fig. 4. Depletion of PC increases autophagy and lipid metabolism activity in an IRE-1-dependent manner. (A–D) Bar plot of the GO analysis of genes upregulated (blue) and downregulated (yellow) in WT (A), *atf-6(lof)* (B), *ire-1(lof)* (C) and *pek-1(lof)* (D) subjected to *pmt-2* RNAi and compared to their respective untreated strains (empty vector). Genes are highlighted in yellow in Table S5. (E) Volcano plot depicting changes in gene expression during UPR^{LBS}. Log_2 gene fold changes are plotted against negative log_{10} FDR P values. Genes that are upregulated or downregulated by more than 1.5-fold and with a FDR<0.05 are labelled with cyan circles. Autophagic (open circles) genes regulated in an IRE-1-dependent manner are shown in black.

Journal of Cell Science (2018) 131, jcs217992. doi:10.1242/jcs.217992

orthologue of human Beclin1, involved in vesicle nucleation) and *wdfy-3* (the orthologue of human WDFY3, an autophagy adaptor) (Melendez et al., 2003; Takacs-Vellai et al., 2005; Jia et al., 2007; Wang et al., 2018). Additionally, the screen identified potential autophagy-related genes that are less characterised and may prompt further investigation. These include *rsks-1* (the orthologue of human RPS6KB1, a negative regulator of autophagy), *sepa-1* (no human orthologue identified, involved in P-granule-associated autophagy) and *trpp-8* (orthologue of human GSG1, involved in autophagic processes) (Silvestrini et al., 2018; Zhang et al., 2009; Meiling-Wesse et al., 2005).

To better understand the crosstalk between UPR^{LBS} and autophagy, we monitored the transcription levels of key genes involved in the regulation of autophagy. Both *bec-1* and *lgg-1* (an orthologue of human MAP1LC3 proteins, involved in autophagosome formation) genes were found to be significantly upregulated in WT, *atf-6(lof)* and *pek-1(lof)* animals, but not in *ire-1(lof)* animals, compared to the control upon *pmt-2* RNAi treatment (Fig. 5B,C). These results suggest that IRE-1 modulates *bec-1* and *lgg-1* expression during LBS. We validated that *bec-1* and *lgg-1* are both upregulated by Tm as previously reported (Ogata et al., 2006). Once IRE-1 is activated, it cleaves *xbp-1* mRNA through an unconventional splicing process. This is followed by the translation of the XBP-1 transcription factor, which regulates a downstream signalling cascade (Walter and Ron, 2011; Ho et al., 2018) that modulates the expression of target genes, including *hsp-3*, during UPR^{LBS} (Fig. S6A). Thus, we monitored *bec-1* and *lgg-1* mRNA levels in *xbp-1(lof)* animals treated with *pmt-2* RNAi. The upregulation of *bec-1* and *lgg-1* was abolished in *xbp-1(lof)* animals suggesting that XBP-1 modulates autophagy during UPR^{LBS} (Fig. 5D,E). Similar increases in the mRNA level of *atg-18* (an orthologue of human *WIPI* genes) and *epg-4* (an orthologue of human *EI24*) were observed in *pmt-2(RNAi)* but not in *xbp-1(lof); pmt-2(RNAi)* animals (Fig. 5F,G) (Tian et al., 2010; Devkota et al., 2016). On the other hand, no significant transcriptional variations in *atg-4.1* (an orthologue of the human *ATG4* genes) and *atg-9* (orthologue of human *ATG9*) were observed, while *atg-16.2* (an orthologue of human *ATG16L1*) was upregulated upon LBS in a XBP-1-independent manner (Fig. S6B–D). Taken together, these findings suggest that the UPR programme transcriptionally regulates a subset of autophagy genes during LBS.

To gain insight into autophagy flux, we used the autophagy reporter strain *plgg-1::gfp::lgg-1* crossed to the RNAi-sensitive *eri-1* worms for simultaneous treatment with *pmt-2* and *ire-1* RNAis (Melendez et al., 2003). We detected an increased number of GFP::LGG-1 puncta in intestinal tissues of *pmt-2(RNAi)* animals, but not in *ire-1* and *pmt-2* double RNAi-treated animals (Fig. 5H,I, Fig. S6E–G). These puncta are indicative of autophagosomes, because spermidine treatment increased their number (Jia et al., 2009). Next, we separated GFP::LGG-1 from its PE-conjugated form, GFP::LGG-1–PE, an autophagosomal marker (Kang et al., 2007). When entering the lysosome, GFP::LGG-1–PE is hydrolysed, releasing stable and free GFP (Hosokawa et al., 2006). Significant increases in GFP::LGG-1–PE as well as free GFP were observed in *pmt-2(RNAi)* but not in *ire-1(RNAi)*; *pmt-2(RNAi)* animals (Fig. 5J,K). Taken together, these results indicate that autophagy is modulated by the IRE-1–XBP-1 axis upon UPR^{LBS}.

DISCUSSION

Lipid perturbation refers to excessive accumulation of lipids in tissues, including liver, pancreas and adipose tissue (Hotamisligil and Erbay, 2008; Rinella and Sanyal, 2015). Dysfunctional UPR and apoptotic pathways resulting from this lipotoxicity ultimately lead to disease outcomes. To better understand the role of the UPR during LBS and the consequence of a compromised UPR programme, several studies have been conducted, focusing on their interconnection. As it is required for normal FA synthesis, as well as the regulation of very low-density lipoprotein (VLDL) assembly and its secretion, *Xbp1* ablation leads to hypolipidemia in mice owing to an abnormal decrease in plasma levels of TG and cholesterol (Lee et al., 2008; So et al., 2012; Wang et al., 2012). High dietary carbohydrate is sufficient to increase FA and cholesterol synthesis through XBP1 (Lee et al., 2008). Consequently, XBP1 is required to channel excess carbohydrate into lipids, as its absence leads to insulin resistance in obese mice (Ozcan et al., 2004). XBP1 is also required to modulate phospholipid synthesis in order to expand the ER membrane network during proteotoxic stress, a process that is proposed to accommodate the increased load of misfolded proteins (Sriburi et al., 2004). The UPR modulates lipid metabolism-related genes, and the absence of its sole regulator in yeast, Ire1, confers auxotrophy of inositol, a building block of phospholipids (Cox et al., 1993). We have previously shown that Ire1 is essential for cell survival during LBS, thereby highlighting the important role of the UPR to overcome lipotoxicity in yeast (Thibault et al., 2012). The UPR sensor PERK also plays a role in pathogenesis from lipotoxicity. Lipotoxicity-induced CHOP (also known as DDIT3), the downstream target gene of PERK, promotes hepatic inflammation by activating the NK-κB pathway, thus promoting NASH and type 2 diabetes (Cunha et al., 2008; Willy et al., 2015). The ablation of ATF6, the third UPR sensor, induces NASH owing to dysregulated lipid biosynthesis in mice upon Tm treatment (Yamamoto et al., 2010). Thus, the three branches of the UPR are intimately linked to lipid homeostasis but their respective roles during lipid bilayer stress in comparison to proteotoxic stress remain elusive. Here, we took a systematic global approach to determine genes that are regulated by the UPR- specifically induced by LBS.

To introduce LBS in *C. elegans*, we opted to genetically attenuate *pmt-2*, which is required for *de novo* PC biosynthesis (Fig. 1A). A similar approach has been used by other groups to mimic the physiological conditions associated with NAFLD in *C. elegans* (Walker et al., 2011; Ding et al., 2015; Smulan et al., 2016). Because both are required for *de novo* PC biosynthesis, *pmt-2* and *sams-1* depletion leads to enlarged lipid droplets in worms (Li et al., 2004). Generally, perturbing PC levels affects the abundance and size of lipid droplets, serving as a compensatory response to LBS that results in the channelling of excess neutral lipids, triacylglycerol and sterol into lipid droplets (LDs) (Guo et al., 2008; Li et al., 2011; Walker et al., 2011).

Decreased hepatic PC in mice (Walkey et al., 1998; Ozcan et al., 2004; Li et al., 2006; Fu et al., 2011) and dietary deficiency of choline in humans are both associated with hepatic steatosis (Buchman et al., 1995; Gao et al., 2016). Initially, we subjected young adult worms to *pmt-2* RNAi for 2 days. However, no significant decrease in PC level was observed (data not shown). This could be due to the slow turnover of phospholipids in *C. elegans*. The absence of cell division in adult worms might not require the rapid synthesis of new membrane lipids, thus genetic ablation of *pmt-2* may have little or no effect on PC levels (Kipreos, 2005). Thus, L1 stage worms treated with *pmt-2* RNAi were utilised as the UPR^{LBS} model. These latter conditions were sufficient to drastically induce LBS, lipid storage and to strongly activate the UPR, all hallmarks of NAFLD (Figs 1 and 2, Figs S1–S3). By using this approach, we interrogated the role of each UPR branch during LBS-induced ER stress.

We employed *C. elegans* for its well-conserved UPR pathways and relative simplicity for genetic analysis. We examined the

Journal of Cell Science (2018) 131, jcs217992. doi:10.1242/jcs.217992

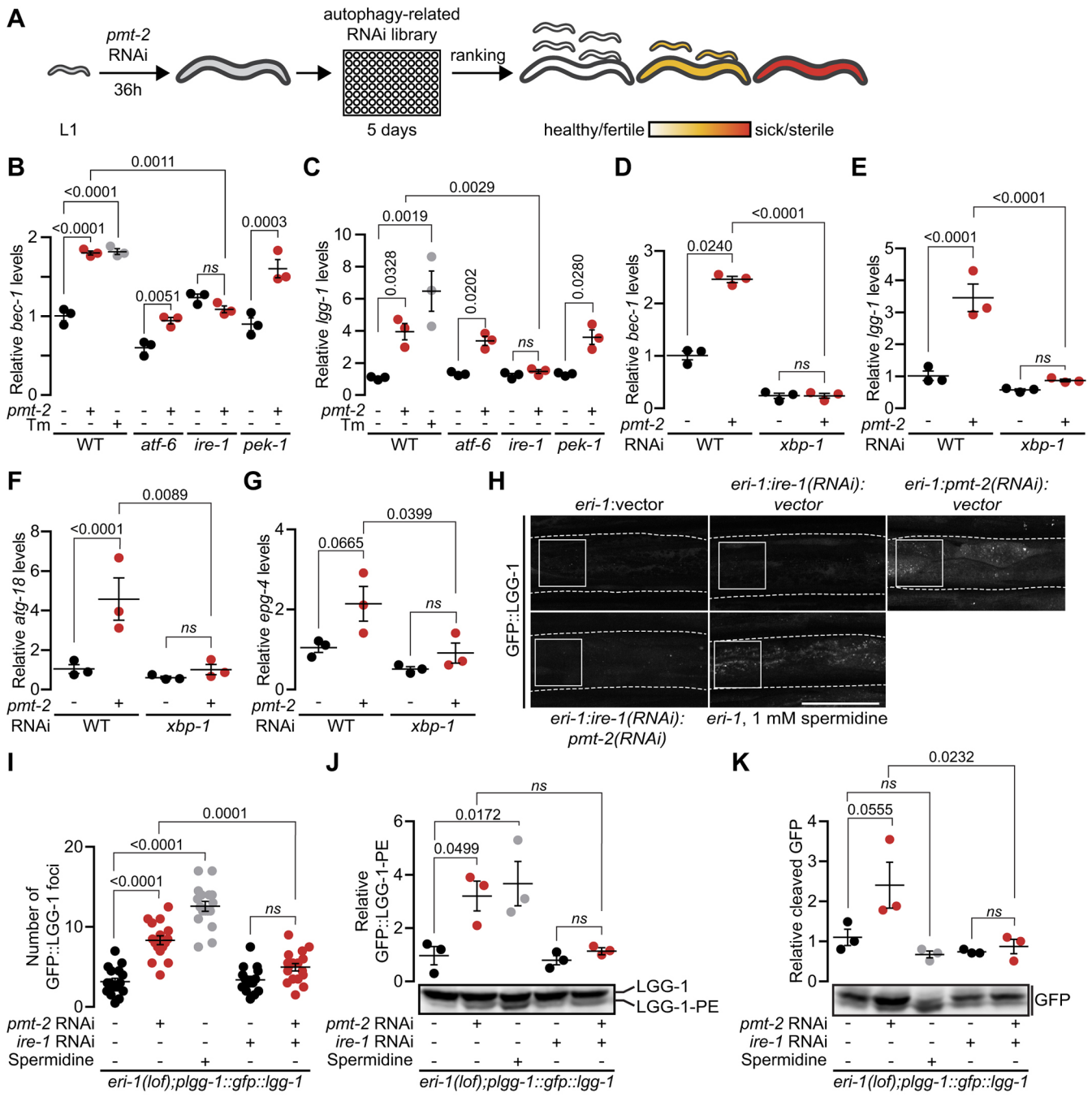

Fig. 5. A subset of autophagy genes is regulated through the IRE-1–XBP-1 axis upon lipid bilayer stress-induced UPR. (A) Schematic representation of the RNAi screening to identify potential autophagy genes that participate in LBS. WT worms were treated with *pmt-2* RNAi for 36 h and subsequently transferred to 96-well plates containing RNAi targeting autophagy-related target genes. Worms were scored for growth defects, sterility, mobility and embryonic lethality. (B–G) qPCR comparing expression of *bec-1* (B) and *lgg-1* (C) in WT, *atf-6(lof)*, *ire-1(lof)* and *pek-1(lof)* worms. qPCR comparing expression of *bec-1* (D), *lgg-1* (E), *atg-18* (F), and *epg-4* (G) in WT and *xbp-1(lof)* animals treated with *pmt-2* RNAi. (H,I) Representative fluorescence images (H) and quantification of GFP::LGG-1 puncta (I) in the anterior intestines of *eri-1;plgg-1::gfp::lgg-1* worms treated for 48 h with *pmt-2* RNAi, *ire-1* RNAi, 1 mM spermidine or a combination of *ire-1* and *pmt-2* RNAis. The box outlined with a solid line depicts the quantification areap; the box outlined with the dashed lines shows the outline of worms. Scale bar: 50 µm. *n*=17, *n*=16, *n*=17, *n*=15, *n*=18, for *eri-1*:vector, *eri-1:pmt-2(RNAi)*, *eri-1* treated with 1 mM spermidine, *eri-1:ire-1(RNAi)*, *eri-1:ire-1(RNAi):pmt-2(RNAi),* respectively. (J,K) Separation of GFP::LGG-1-PE (J) and cleaved GFP (K) in *eri-1;plgg-1::gfp::lgg-1* worm lysate treated as in H and I. The lysates were prepared and analysed by immunoblotting with anti-GFP antibodies and normalised to total protein loading control (Fig. S6H). The amount of cleaved GFP is indicative of the amount of autophagic flux because the GFP degradation takes place at the autolysosomes. As a measure of autophagic flux, ratios of GFP::LGG-1-PE to total protein and of cleaved GFP to total proteins were compared. Data shown are the mean±s.e.m. of at least three independent experiments. Statistical analysis was subjected to one-way ANOVA followed by Tukey's multiple comparisons adjustment. ns, not significant.

individual effects of *atf-6*, *ire-1* and *pek-1* deficiency *in vivo*. Interestingly, ER stress induced by unfolded protein accumulation and LBS were found to be distinct from each other (Hou et al., 2014; Lajoie et al., 2012). A global transcriptomic analysis of UPR mutants subjected to LBS in comparison to what was seen with proteotoxic-induced ER stress in WT animals allowed us to identify

Journal of Cell Science (2018) 131, jcs217992. doi:10.1242/jcs.217992

genes that were specifically regulated by UPR^{LBS} but not UPR^{PT} (Fig. 3). To our knowledge, this is the first report identifying specific UPR-regulated genes induced by LBS but not proteotoxic stress. Our data show that a number of genes regulated by the UPR transducers are specific to LBS, while a smaller number of genes are commonly modulated under proteotoxic and lipid stress. As expected, LBS-induced ER stress leads to altered gene regulation and protein modification processes through ATF-6, IRE-1 and PEK-1 (Figs 3 and 4). IRE-1 is the most-conserved UPR transducer from yeast to mammals, and it regulates the largest number of genes among the three UPR transducers (Fig. 3B).

Our autophagy screening revealed that autophagy is essential during LBS, suggesting that it has an important role in regulating lipid metabolism. The change in cellular lipid landscape is at least partially mediated by autophagy through the IRE-1–XBP-1 axis (Figs 4 and 5). Generally considered a cytoprotective response, autophagy can be modulated by ER stress. PERK has been reported to modulate autophagy by phosphorylating eIF2α, resulting in a general translational inhibition (Matsumoto et al., 2013; Avivar-Valderas et al., 2011; Fujita et al., 2007; Kouroku et al., 2007). In parallel, PERK has also been reported to regulate autophagy through the transcription factor ATF4 (an orthologue of ATF-5) (Carra et al., 2009; Dever, 2002; Talloczy et al., 2002). Likewise, IRE1 modulates autophagy independently of XBP1, by activating the Jun N-terminal kinase (JNK) pathway (Younce and Kolattukudy, 2012; Vidal et al., 2012; Pattingre et al., 2009; Wei et al., 2008a,b; Ogata et al., 2006). Autophagy has additionally been reported to be activated (Younce and Kolattukudy, 2012) or inhibited (Vidal et al., 2012) by the IRE1–XBP1 axis (Adolph et al., 2013; Zhao et al., 2013; Hetz et al., 2009).

Muting the UPR during LBS revealed that the IRE-1–XBP-1 axis specifically modulates autophagy (Fig. 6). Our findings also demonstrate that a subset of autophagy genes is essential for organismal health during LBS (Fig. 5A; Fig. S5, Table S6).

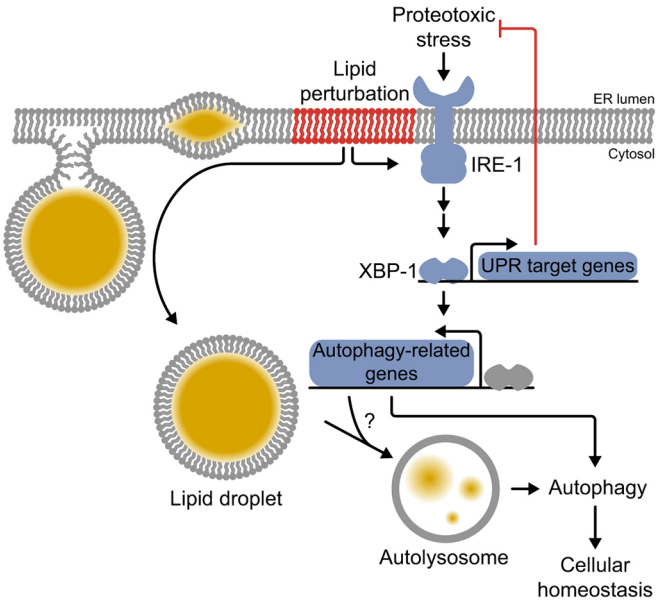

Fig. 6. UPR^{LBS} regulates autophagy through the canonical IRE-1/XBP-1 UPR branch. Proteotoxic-induced ER stress activates a subset of UPR target genes to restore ER homeostasis. In addition, LBS-induced ER stress partially induces autophagy through the IRE-1–XBP-1 axis. Intact of autophagy function during proteotoxic or LBS is essential in maintaining cellular homeostasis and contributes to organismal health.

Considering the important role of lipid homeostasis and how its impairment contributes to the pathology of metabolic diseases, our data revealed the important role of a functional UPR programme to regulate autophagy and, consequently, maintain cellular homeostasis. As increasing evidence suggests that reduced levels of autophagy contribute to a myriad of pathological outcomes (Mizushima et al., 2008; Singh et al., 2009), the autophagy process might be a useful target for therapeutic strategies in metabolic diseases.

MATERIALS AND METHODS

C. elegans strains and RNAi constructs

All strains were grown at 20°C using standard *C. elegans* methods as previously described (Brenner, 1974; Stiernagle, 2006). Nematode growth medium (NGM) agar plates were seeded with *E. coli* strain OP50 for normal growth and with HT115 bacteria for RNAi feeding. RNAi feeding was performed as previously described (Timmons and Fire, 1998), and the RNAi library was obtained from the Fire laboratory (purchased through Dharmacon, Lafayette, CO) (Fire et al., 1998). The plasmids were sequenced to confirm their identity. Wild-type N2 Bristol, *atf-6*(ok551), *ire-1*(ok799), *pek-1*(ok275), *pmt-2*(vc1952), *phsp4::gfp*(sj4005), *xbp-1(lof);phsp-4::gfp*(sj17), *eri-1(mg366)* and *plgg-1::gfp::lgg-1*(adIs2122) strains were obtained from *Caenorhabditis* Genetic Center (CGC). The *eri-1:plgg-1::gfp::lgg-1* reporter strain was obtained by crossing *eri-1* worms to *plgg-1::gfp::lgg-1* as previously described (Fay, 2006).

RNAi by feeding

RNAi was carried out as previously described (Timmons and Fire, 1998). Briefly, HT115 bacteria harbouring pL4440 plasmids were grown in LB medium containing 100 µg/ml ampicillin at 37°C until log phase [optical density at 600 nm (OD_{600}) of 0.6] and seeded onto NGM agar plates containing 50 µg/ml carbenicillin and 1 mM isopropyl β-D-1-thiogalactopyranoside (IPTG). Gravid adult worms were treated with hypochlorite and eggs were hatched overnight in M9 medium at 20°C to obtain L1 synchronised worms. Hatched L1 larvae were transferred to RNAi agar plates and grown until L4 larval to young adult stages. L4/young adult worms were harvested and incubated with 25 µg/ml Tm in M9 medium for 4 h at 20°C followed by washes with M9 when indicated. To measure body length, worms were transferred to 6 cm NGM plates without bacteria. Bright-field images were acquired with a dissecting microscope (Nikon SMZ1500) fitted with a JVC digital camera at 100× magnification. Length measurements were performed in Fiji software with the WormSizer plugin (Moore et al., 2013). For double-RNAi feeding, worms were fed with equal amount of HT115 bacteria harbouring pL4440 plasmids and the efficacy of gene silencing was assessed by qPCR.

qPCR

L4/young adult worms (~10,000) were collected, resuspended in water and lysed with a motorised pestle homogeniser. Total RNA was isolated using TRIzol reagent (Thermo Fisher, Waltham, MA) and subsequently purified using RNeasy Mini (Qiagen, Venlo, Netherlands) columns following the manufacturer's protocols. DNase treatment in columns was carried out with RNase-free DNase (Qiagen, Venlo, Netherlands) following the manufacturer's protocol. cDNA was synthesised from 2 µg of total RNA using RevertAid reverse transcriptase (Thermo Fisher, Waltham, MA) following manufacturer's protocol. SYBR Green qPCR experiments were performed following the manufacturer's protocol using a QuantStudio 6 Flex Real-time PCR system (Applied Biosystems, Waltham, MA). cDNA (30 ng) and 50 nM of paired-primer mix were used for each reaction. Relative mRNA was determined with the comparative Ct method (ΔΔCt) normalised to housekeeping gene *act-1*. Oligonucleotide primers used are listed in Table S1.

Lipid extraction and phospholipid analysis

L4/young adult worms (~10,000) were harvested and washed thoroughly with M9 buffer, lysed with 1 mm silica beads by bead beating and subsequently lyophilised overnight (Virtis). All subsequent steps were carried out at 4°C. Total lipids were extracted from dried samples with chloroform:methanol

(2:1) and concentrated. Total lipid extracts and POPE (1-palmitoyl-2-oleoyl-sn-glycero-3-phosphoethanolamine; 16:0-18:1n9 PE; Avanti Polar Lipids, Alabaster, AL)/DOPC (1,2-dioleoyl-sn-glycero-3-phosphocholine; 18:1n9 PC; Avanti Polar Lipids, Alabaster, AL) standard mix were spotted on HPTLC Silica gel 60 plates using Linomat 5 (CAMAG) and separated with chloroform:methanol:acetic acid:acetone:water (35:25:4:14:2). Phospholipids were visualised under long-wave ultraviolet light (λ=340 nm) by spraying 0.05 mg/ml of Primuline dye in acetone:water (80:20) onto the dried plates. Spots corresponding to PE and PC were scraped off the silica plates and transferred into 2 ml glass tubes. A 100 µl volume of 1 mM C15:0 (pentadecanoic acid) was added to the tubes containing silica-bound phospholipids as an internal standard. The phospholipids were hydrolysed and esterified to fatty acid methyl esters (FAME) with 300 µl of 1.25 M HCl-methanol for 1 h at 80°C. FAMEs were extracted three times with 1 ml of hexane. Combined extracts were dried under nitrogen, and resuspended in 100 µl hexane. FAMEs were separated by gas chromatography with a flame ionisation detector (GC-FID) (GC-2014, Shimadzu, Kyoto, Japan) using an ULBON HR-SS-10 50 m×0.25 mm column (Shinwa, Tokyo, Japan). Supelco 37 component FAME mix was used to identify corresponding FAs (Sigma-Aldrich, St Louis, MO). Data were normalised using the internal standard C15:0 and worm dry mass.

Lipid droplets analysis by means of Sudan Black

Following RNAi feeding, lipid droplets of L4 worms were stained with Sudan Black B (Sigma-Aldrich, St Louis, MO) as described previously with a few modifications (Ogg and Ruvkun, 1998). Briefly, worms were fixed in 1% paraformaldehyde in M9 buffer for 30 min at room temperature, followed by three freeze-thaw cycles using liquid nitrogen. Worms were washed once with M9 and gradually dehydrated with 25%, 50% and 70% ethanol. Subsequently, fixed worms were stained with 50% saturated Sudan Black B in 70% ethanol (filtered with a 0.22 µm membrane) for 30 min at room temperature with rocking. Stained worms were washed once with 25% ethanol for 30 min with rocking. Worms were mounted on a 2% agarose pads for imaging. Bright-field images of worms were taken with a DMi8 inverted epifluorescence microscope (Leica, Wetzlar, Germany) with 20× and 63× objective lenses. To quantify the number and size of lipid droplets, TIFF images taken at 63× magnification were converted to 8-bit grayscale images, followed by background subtraction and thresholding with Fiji imaging software. Lipid droplets were divided into three size groups based on the diameter of LDs: small (0.8–3 µm), medium (3.1-6 µm) and large (>6 µm). The percentage of LDs per size group as a proportion of the number of measured LDs per condition was presented.

Spermidine treatment

Worms at L4 stage were collected in M9 buffer and treated with 1 mM spermidine (Sigma-Aldrich) for 16 h at 20°C with shaking. Worms were then washed three times with M9 buffer and harvested for downstream experiments.

Immunoblotting

Worms were collected, washed in M9 buffer and subsequently lysed in RIPA buffer (50 mM Tris-HCl pH 7.5, 150 mM NaCl, 1% NP-40, 0.1% SDS, 2 mM EDTA, and 0.5% sodium deoxycholate) with protease inhibitor cocktail (Roche, Basel, Switzerland) by bead beating three times for 30 s at 6500 rpm with the samples chilled on ice between the homogenisation steps. Samples were then centrifuged at 10,000 ***g*** for 5 min at 4°C to remove debris. Cleared lysate protein concentration was measured by using a BCA assay kit (Thermo Fisher, Waltham, MA). Either 60 µg or 80 µg of total proteins were loaded into 10% SDS-PAGE gels to detect free GFP and GFP::LGG-1, respectively; proteins were transferred to nitrocellulose membranes and stained with REVERT total protein stain (Li-COR Biosciences, Lincoln, NE) for normalisation. Membranes were blocked for 1 h with Odyssey blocking buffer TBS (Li-COR Biosciences, Lincoln, NE) at room temperature, and incubated with 1:1000 of monoclonal anti-GFP antibody overnight at 4°C (Roche, catalogue number 11814460001), washed, and incubated with 1:10,000 of IRDye 800CW anti-mouse IgG antibody (Li-COR Biosciences, Lincoln, NE, catalogue number 925-32210). Membranes were washed and scanned with an Odyssey CLx imaging system (Li-COR Biosciences, Lincoln, NE).

Quantification of autophagic vesicles

To quantify autophagic vesicles, *eri-1;lgg-1p::gfp::lgg-1* worms were immobilised in M9 containing 0.5 M NaN_3 and mounted on 2% agarose pad and imaged using LSM Zeiss 710 scanning confocal microscope (Zeiss, Oberkochen, Germany). GFP excitation and emission wavelengths were adjusted to 493 and 517 nm, respectively, to reduce autofluorescence. *Z*-stacks were acquired with a 63× objective of 0.6 µm thickness. Line average scanning was set to eight times to increase the signal-to-noise ratio. Maximum intensity projections were acquired from the *z*-stack images with ZEN software (Zeiss, Oberkochen, Germany). The number of GFP-positive puncta were quantified in one 1000 μm^2 area around the anterior intestines with ZEN software.

DNA microarray

Three independent populations of WT, *atf-6(lof)*, *ire-1(lof)*, *pek-1(lof)* and *pmt-2(lof)* worms were synchronised via hypochlorite treatment. L1 stage animals were treated with *pmt-2* RNAi or pL4440 empty vector for 48 h. Next, total RNA from the treated worms was isolated as described above. RNA quality control for microarray analysis was carried out using a Agilent 2100 Bioanalyzer (Agilent Technologies, Santa Clara, CA). RNA samples with a RIN score >9.5 were deemed suitable for microarrays. The cDNAs were then synthesised from 100 ng of total RNA, purified, fragmented and hybridised to GeneChip *C. elegans* Gene 1.0 ST arrays. Differentially expressed genes were identified by using Affymetrix Transcriptome Analysis Console (TAC) 3.0 software. The threshold for selecting differentially expressed genes was set at a difference of more than 1.5 fold with *P*-values lower than 0.05 obtained by one-way ANOVA testing. GOrilla (http://cbl-gorilla.cs.technion.ac.il/) (Eden et al., 2009), REViGO (http://revigo.irb.hr/) (Supek et al., 2011) and DAVID (https://david.ncifcrf.gov/) (Huang et al., 2007) were used for GO terms analysis. Heat maps in the figures were generated using R Studio. Venn diagrams were generated using the following generator (http://bioinfo.genotoul.fr/jvenn/example.html). For gene expression analysis, normalised and log-transformed array data were imported to Cluster 3.0 for fold cut-off and hierarchical clustering. Genes were filtered to obtain those with a significant change in gene expression (fold change >1.5 between RNAi-treated and untreated samples at $P<0.05$). The filtered data set was hierarchically clustered based on average linkage and the Pearson correlation method, and the output was displayed in TreeView. qPCR was performed to verify mRNA expression of selected gene targets.

RNAi screening of autophagy-related genes

RNAi screen was carried out as previously described with minor modifications (Lehner et al., 2006). Briefly, L1 larval stage animals were synchronised by hypochlorite treatment and exposed to *pmt-2* RNAi on NGM agar plates for 36 h. Thereafter, worms were washed three times with M9 and five to ten worms were seeded into a 96-well plate containing RNAi clones to inhibit genes with autophagy-related functions. Control RNAi plates comprised worms exposed to pL4440 empty vector for 48 h and subsequently seeded into 96-well plates containing the same RNAi clones as above. Phenotypes of the worms were monitored over a 5-day period. Phenotypes were compared to control RNAi plates where the worms were scored for sterility and reduced body size semi-quantitatively on a scale from 0 (wild-type) to 2 (100% sterility or stunted growth) (Lehner et al., 2006).

Statistics

Error bars indicate standard error of the mean (s.e.m.), calculated from at least three biological replicates, unless otherwise indicated. *P*-values were calculated using a one-way ANOVA with Tukey's post hoc test, unless otherwise indicated and reported as *P*-values with four significant digits in the figures. All statistical tests were performed using GraphPad Prism 7 software.

Acknowledgements

We are grateful to Drs Fumio Motegi, Jean-Claude Labbé and Ronen Zaidel-Bar for providing reagents and technical support to introduce *C. elegans* as a new model system in the laboratory. Some strains were provided by the CGC, which is funded by NIH Office of Research Infrastructure Programs (P40 OD010440). We thank Peter Shyu Jr. for critical reading of the manuscript.

Competing interests
The authors declare no competing or financial interests.

Author contributions
Conceptualization: G.T.; Methodology: J.H.K., L.W., C.B.-C., G.T.; Formal analysis: J.H.K.; Investigation: J.H.K., L.W., C.B.-C.; Resources: J.H.K., L.W.; Writing - original draft: J.H.K., G.T.; Writing - review & editing: J.H.K., L.W., C.B.-C., G.T.; Supervision: G.T.; Project administration: G.T.; Funding acquisition: J.H.K., G.T.

Funding
This work was supported by the Nanyang Assistant Professorship programme from the Nanyang Technological University, the Ministry of Education - Singapore Academic Research Fund Tier 1 (2016-T1-001-078), and the Nanyang Technological University Research Scholarship to J.H.K. (predoctoral fellowship).

Data availability
The DNA microarray data discussed in this publication was deposited in the NCBI Gene Expression Onmibus (GEO) database under accession number GSE99763.

Supplementary information
Supplementary information available online at
http://jcs.biologists.org/lookup/doi/10.1242/jcs.217992.supplemental

References
Acosta-Alvear, D., Zhou, Y., Blais, A., Tsikitis, M., Lents, N. H., Arias, C., Lennon, C. J., Kluger, Y. and Dynlacht, B. D. (2007). XBP1 controls diverse cell type- and condition-specific transcriptional regulatory networks. *Mol. Cell* **27**, 53-66.

Adolph, T. E., Tomczak, M. F., Niederreiter, L., Ko, H. J., Bock, J., Martinez-Naves, E., Glickman, J. N., Tschurtschenthaler, M., Hartwig, J., Hosomi, S. et al. (2013). Paneth cells as a site of origin for intestinal inflammation. *Nature* **503**, 272-276.

Agouni, A., Mody, N., Owen, C., Czopek, A., Zimmer, D., Bentires-Alj, M., Bence, K. K. and Delibegovic, M. (2011). Liver-specific deletion of protein tyrosine phosphatase (PTP) 1B improves obesity- and pharmacologically induced endoplasmic reticulum stress. *Biochem. J.* **438**, 369-378.

Arendt, B. M., Ma, D. W., Simons, B., Noureldin, S. A., Therapondos, G., Guindi, M., Sherman, M. and Allard, J. P. (2013). Nonalcoholic fatty liver disease is associated with lower hepatic and erythrocyte ratios of phosphatidylcholine to phosphatidylethanolamine. *Appl. Physiol. Nutr. Metab.* **38**, 334-340.

Avivar-Valderas, A., Salas, E., Bobrovnikova-Marjon, E., Diehl, J. A., Nagi, C., Debnath, J. and Aguirre-Ghiso, J. A. (2011). PERK integrates autophagy and oxidative stress responses to promote survival during extracellular matrix detachment. *Mol. Cell. Biol.* **31**, 3616-3629.

Bettaieb, A., Matsuo, K., Matsuo, I., Wang, S., Melhem, R., Koromilas, A. E. and Haj, F. G. (2012). Protein tyrosine phosphatase 1B deficiency potentiates PERK/eIF2alpha signaling in brown adipocytes. *PLoS ONE* **7**, e34412.

Braakman, I. and Bulleid, N. J. (2011). Protein folding and modification in the mammalian endoplasmic reticulum. *Annu. Rev. Biochem.* **80**, 71-99.

Brendza, K. M., Haakenson, W., Cahoon, R. E., Hicks, L. M., Palavalli, L. H., Chiapelli, B. J., Mclaird, M., Mccarter, J. P., Williams, D. J., Hresko, M. C. et al. (2007). Phosphoethanolamine N-methyltransferase (PMT-1) catalyses the first reaction of a new pathway for phosphocholine biosynthesis in Caenorhabditis elegans. *Biochem. J.* **404**, 439-448.

Brenner, S. (1974). The genetics of Caenorhabditis elegans. *Genetics* **77**, 71-94.

Buchman, A. L., Dubin, M. D., Moukarzel, A. A., Jenden, D. J., Roch, M., Rice, K. M., Gornbein, J. and Ament, M. E. (1995). Choline deficiency: a cause of hepatic steatosis during parenteral nutrition that can be reversed with intravenous choline supplementation. *Hepatology* **22**, 1399-1403.

Calfon, M., Zeng, H., Urano, F., Till, J. H., Hubbard, S. R., Harding, H. P., Clark, S. G. and Ron, D. (2002). IRE1 couples endoplasmic reticulum load to secretory capacity by processing the XBP-1 mRNA. *Nature* **415**, 92-96.

Carra, S., Brunsting, J. F., Lambert, H., Landry, J. and Kampinga, H. H. (2009). HspB8 participates in protein quality control by a non-chaperone-like mechanism that requires eIF2{alpha} phosphorylation. *J. Biol. Chem.* **284**, 5523-5532.

Cox, J. S. and Walter, P. (1996). A novel mechanism for regulating activity of a transcription factor that controls the unfolded protein response. *Cell* **87**, 391-404.

Cox, J. S., Shamu, C. E. and Walter, P. (1993). Transcriptional induction of genes encoding endoplasmic reticulum resident proteins requires a transmembrane protein kinase. *Cell* **73**, 1197-1206.

Cunha, D. A., Hekerman, P., Ladriere, L., Bazarra-Castro, A., Ortis, F., Wakeham, M. C., Moore, F., Rasschaert, J., Cardozo, A. K., Bellomo, E. et al. (2008). Initiation and execution of lipotoxic ER stress in pancreatic beta-cells. *J. Cell Sci.* **121**, 2308-2318.

Dever, T. E. (2002). Gene-specific regulation by general translation factors. *Cell* **108**, 545-556.

Devkota, S., Jeong, H., Kim, Y., Ali, M., Roh, J. I., Hwang, D. and Lee, H. W. (2016). Functional characterization of EI24-induced autophagy in the degradation of RING-domain E3 ligases. *Autophagy* **12**, 2038-2053.

Ding, W., Smulan, L. J., Hou, N. S., Taubert, S., Watts, J. L. and Walker, A. K. (2015). s-Adenosylmethionine levels govern innate immunity through distinct methylation-dependent pathways. *Cell Metab.* **22**, 633-645.

Dowd, S. R., Bier, M. E. and Patton-Vogt, J. L. (2001). Turnover of phosphatidylcholine in Saccharomyces cerevisiae. The role of the CDP-choline pathway. *J. Biol. Chem.* **276**, 3756-3763.

Doycheva, I., Watt, K. D., Rifai, G., Abou Mrad, R., Lopez, R., Zein, N. N., Carey, W. D. and Alkhouri, N. (2017). Increasing burden of chronic liver disease among adolescents and young adults in the USA: a silent epidemic. *Dig. Dis. Sci.* **62**, 1373-1380.

Eden, E., Navon, R., Steinfeld, I., Lipson, D. and Yakhini, Z. (2009). GOrilla: a tool for discovery and visualization of enriched GO terms in ranked gene lists. *BMC Bioinformatics* **10**, 48.

Ericson, M. C., Gafford, J. T. and Elbein, A. D. (1977). Tunicamycin inhibits GlcNAc-lipid formation in plants. *J. Biol. Chem.* **252**, 7431-7433.

Fay, D. (2006). Genetic mapping and manipulation: chapter 1–Introduction and basics. *WormBook* 1-12.

Fire, A., Xu, S., Montgomery, M. K., Kostas, S. A., Driver, S. E. and Mello, C. C. (1998). Potent and specific genetic interference by double-stranded RNA in Caenorhabditis elegans. *Nature* **391**, 806-811.

Fu, S., Yang, L., Li, P., Hofmann, O., Dicker, L., Hide, W., Lin, X., Watkins, S. M., Ivanov, A. R. and Hotamisligil, G. S. (2011). Aberrant lipid metabolism disrupts calcium homeostasis causing liver endoplasmic reticulum stress in obesity. *Nature* **473**, 528-531.

Fujita, E., Kouroku, Y., Isoai, A., Kumagai, H., Misutani, A., Matsuda, C., Hayashi, Y. K. and Momoi, T. (2007). Two endoplasmic reticulum-associated degradation (ERAD) systems for the novel variant of the mutant dysferlin: ubiquitin/proteasome ERAD(I) and autophagy/lysosome ERAD(II). *Hum. Mol. Genet.* **16**, 618-629.

Gao, X., Wang, Y., Randell, E., Pedram, P., Yi, Y., Gulliver, W. and Sun, G. (2016). Higher dietary choline and betaine intakes are associated with better body composition in the adult population of newfoundland, canada. *PLoS ONE* **11**, e0155403.

Guo, Y., Walther, T. C., Rao, M., Stuurman, N., Goshima, G., Terayama, K., Wong, J. S., Vale, R. D., Walter, P. and Farese, R. V. (2008). Functional genomic screen reveals genes involved in lipid-droplet formation and utilization. *Nature* **453**, 657-661.

Halbleib, K., Pesek, K., Covino, R., Hofbauer, H. F., Wunnicke, D., Hanelt, I., Hummer, G. and Ernst, R. (2017). Activation of the unfolded protein response by lipid bilayer stress. *Mol. Cell* **67**, 673-684 e8.

Han, J. and Kaufman, R. J. (2016). The role of ER stress in lipid metabolism and lipotoxicity. *J. Lipid Res.* **57**, 1329-1338.

Harding, H. P., Zhang, Y., Zeng, H., Novoa, I., Lu, P. D., Calfon, M., Sadri, N., Yun, C., Popko, B., Paules, R. et al. (2003). An integrated stress response regulates amino acid metabolism and resistance to oxidative stress. *Mol. Cell* **11**, 619-633.

Hetz, C., Thielen, P., Matus, S., Nassif, M., Court, F., Kiffin, R., Martinez, G., Cuervo, A. M., Brown, R. H. and Glimcher, L. H. (2009). XBP-1 deficiency in the nervous system protects against amyotrophic lateral sclerosis by increasing autophagy. *Genes Dev.* **23**, 2294-2306.

Ho, N., Xu, C. and Thibault, G. (2018). From the unfolded protein response to metabolic diseases - lipids under the spotlight. *J. Cell Sci.* **131**.

Hörl, G., Wagner, A., Cole, L. K., Malli, R., Reicher, H., Kotzbeck, P., Köfeler, H., Hofler, G., Frank, S., Bogner-Strauss, J. G. et al. (2011). Sequential synthesis and methylation of phosphatidylethanolamine promote lipid droplet biosynthesis and stability in tissue culture and in vivo. *J. Biol. Chem.* **286**, 17338-17350.

Hosokawa, N., Hara, Y. and Mizushima, N. (2006). Generation of cell lines with tetracycline-regulated autophagy and a role for autophagy in controlling cell size. *FEBS Lett.* **580**, 2623-2629.

Hotamisligil, G. S. and Erbay, E. (2008). Nutrient sensing and inflammation in metabolic diseases. *Nat. Rev. Immunol.* **8**, 923-934.

Hou, N. S., Gutschmidt, A., Choi, D. Y., Pather, K., Shi, X., Watts, J. L., Hoppe, T. and Taubert, S. (2014). Activation of the endoplasmic reticulum unfolded protein response by lipid disequilibrium without disturbed proteostasis in vivo. *Proc. Natl. Acad. Sci. USA* **111**, E2271-E2280.

Huang, D. W., Sherman, B. T., Tan, Q., Collins, J. R., Alvord, W. G., Roayaei, J., Stephens, R., Baseler, M. W., Lane, H. C. and Lempicki, R. A. (2007). The DAVID gene functional classification tool: a novel biological module-centric algorithm to functionally analyze large gene lists. *Genome Biol.* **8**, R183.

Jia, K., Hart, A. C. and Levine, B. (2007). Autophagy genes protect against disease caused by polyglutamine expansion proteins in Caenorhabditis elegans. *Autophagy* **3**, 21-25.

Jia, K., Thomas, C., Akbar, M., Sun, Q., Adams-Huet, B., Gilpin, C. and Levine, B. (2009). Autophagy genes protect against Salmonella typhimurium infection and mediate insulin signaling-regulated pathogen resistance. *Proc. Natl. Acad. Sci. USA* **106**, 14564-14569.

Kang, C., You, Y.-J. and Avery, L. (2007). Dual roles of autophagy in the survival of Caenorhabditis elegans during starvation. *Genes Dev.* **21**, 2161-2171.

Kim, M. H., Aydemir, T. B., Kim, J. and Cousins, R. J. (2017). Hepatic ZIP14-mediated zinc transport is required for adaptation to endoplasmic reticulum stress. *Proc. Natl. Acad. Sci. USA* **114**, E5805-E5814.
Kipreos, E. T. (2005). C. elegans cell cycles: invariance and stem cell divisions. *Nat. Rev. Mol. Cell Biol.* **6**, 766-776.
Kouroku, Y., Fujita, E., Tanida, I., Ueno, T., Isoai, A., Kumagai, H., Ogawa, S., Kaufman, R. J., Kominami, E. and Momoi, T. (2007). ER stress (PERK/eIF2alpha phosphorylation) mediates the polyglutamine-induced LC3 conversion, an essential step for autophagy formation. *Cell Death Differ.* **14**, 230-239.
Lagace, T. A. and Ridgway, N. D. (2013). The role of phospholipids in the biological activity and structure of the endoplasmic reticulum. *Biochim. Biophys. Acta* **1833**, 2499-2510.
Lajoie, P., Moir, R. D., Willis, I. M. and Snapp, E. L. (2012). Kar2p availability defines distinct forms of endoplasmic reticulum stress in living cells. *Mol. Biol. Cell* **23**, 955-964.
Lee, A. H., Scapa, E. F., Cohen, D. E. and Glimcher, L. H. (2008). Regulation of hepatic lipogenesis by the transcription factor XBP1. *Science* **320**, 1492-1496.
Lehner, B., Tischler, J. and Fraser, A. G. (2006). RNAi screens in Caenorhabditis elegans in a 96-well liquid format and their application to the systematic identification of genetic interactions. *Nat. Protoc.* **1**, 1617-1620.
Li, Y., Ge, M., Ciani, L., Kuriakose, G., Westover, E. J., Dura, M., Covey, D. F., Freed, J. H., Maxfield, F. R., Lytton, J. et al. (2004). Enrichment of endoplasmic reticulum with cholesterol inhibits sarcoplasmic-endoplasmic reticulum calcium ATPase-2b activity in parallel with increased order of membrane lipids: implications for depletion of endoplasmic reticulum calcium stores and apoptosis in cholesterol-loaded macrophages. *J. Biol. Chem.* **279**, 37030-37039.
Li, Z., Agellon, L. B. and Vance, D. E. (2005). Phosphatidylcholine homeostasis and liver failure. *J. Biol. Chem.* **280**, 37798-37802.
Li, Z., Agellon, L. B., Allen, T. M., Umeda, M., Jewell, L., Mason, A. and Vance, D. E. (2006). The ratio of phosphatidylcholine to phosphatidylethanolamine influences membrane integrity and steatohepatitis. *Cell Metab.* **3**, 321-331.
Li, Y., Na, K., Lee, H. J., Lee, E. Y. and Paik, Y. K. (2011). Contribution of sams-1 and pmt-1 to lipid homoeostasis in adult Caenorhabditis elegans. *J. Biochem.* **149**, 529-538.
Ling, J., Reynolds, N. and Ibba, M. (2009). Aminoacyl-tRNA synthesis and translational quality control. *Annu. Rev. Microbiol.* **63**, 61-78.
Ling, J., Chaba, T., Zhu, L.-F., Jacobs, R. L. and Vance, D. E. (2012). Hepatic ratio of phosphatidylcholine to phosphatidylethanolamine predicts survival after partial hepatectomy in mice. *Hepatology* **55**, 1094-1102.
Long, X., Spycher, C., Han, Z. S., Rose, A. M., Muller, F. and Avruch, J. (2002). TOR deficiency in C. elegans causes developmental arrest and intestinal atrophy by inhibition of mRNA translation. *Curr. Biol.* **12**, 1448-1461.
Matsumoto, H., Miyazaki, S., Matsuyama, S., Takeda, M., Kawano, M., Nakagawa, H., Nishimura, K. and Matsuo, S. (2013). Selection of autophagy or apoptosis in cells exposed to ER-stress depends on ATF4 expression pattern with or without CHOP expression. *Biol. Open* **2**, 1084-1090.
Meiling-Wesse, K., Epple, U.D., Krick, R., Barth, H., Appelles, A., Voss, C., Eskelinen, E.L. and Thumm, M. (2005). Trs85 (Gsg1), a component of the TRAPP complexes, is required for the organization of the preautophagosomal structure during selective autophagy via the Cvt pathway. *J. Biol. Chem.* **280**, 33669-33678.
Melendez, A., Talloczy, Z., Seaman, M., Eskelinen, E. L., Hall, D. H. and Levine, B. (2003). Autophagy genes are essential for dauer development and life-span extension in C. elegans. *Science* **301**, 1387-1391.
Mizushima, N. and Komatsu, M. (2011). Autophagy: renovation of cells and tissues. *Cell* **147**, 728-741.
Mizushima, N., Levine, B., Cuervo, A. M. and Klionsky, D. J. (2008). Autophagy fights disease through cellular self-digestion. *Nature* **451**, 1069-1075.
Moore, B. T., Jordan, J. M. and Baugh, L. R. (2013). WormSizer: high-throughput analysis of nematode size and shape. *PLoS ONE* **8**, e57142.
Morein, S., Andersson, A., Rilfors, L. and Lindblom, G. (1996). Wild-type Escherichia coli cells regulate the membrane lipid composition in a "window" between gel and non-lamellar structures. *J. Biol. Chem.* **271**, 6801-6809.
Mota, M., Banini, B. A., Cazanave, S. C. and Sanyal, A. J. (2016). Molecular mechanisms of lipotoxicity and glucotoxicity in nonalcoholic fatty liver disease. *Metabolism* **65**, 1049-1061.
Ng, D. T., Spear, E. D. and Walter, P. (2000). The unfolded protein response regulates multiple aspects of secretory and membrane protein biogenesis and endoplasmic reticulum quality control. *J. Cell Biol.* **150**, 77-88.
Ng, B. S. H., Shyu, P. T., Chaw, R., Seah, Y. L. and Thibault, G. (2017). Lipid perturbation compromises UPR-mediated ER homeostasis as a result of premature degradation of membrane proteins. *bioRxiv*, doi:10.1101/178947.
Novoa, I., Zeng, H., Harding, H. P. and Ron, D. (2001). Feedback inhibition of the unfolded protein response by GADD34-mediated dephosphorylation of eIF2alpha. *J. Cell Biol.* **153**, 1011-1022.
Ogata, M., Hino, S.-I., Saito, A., Morikawa, K., Kondo, S., Kanemoto, S., Murakami, T., Taniguchi, M., Tanii, I., Yoshinaga, K. et al. (2006). Autophagy is activated for cell survival after endoplasmic reticulum stress. *Mol. Cell. Biol.* **26**, 9220-9231.
Ogg, S. and Ruvkun, G. (1998). The C. elegans PTEN homolog, DAF-18, acts in the insulin receptor-like metabolic signaling pathway. *Mol. Cell* **2**, 887-893.
Oursel, D., Loutelier-Bourhis, C., Orange, N., Chevalier, S., Norris, V. and Lange, C. M. (2007). Lipid composition of membranes of Escherichia coli by liquid chromatography/tandem mass spectrometry using negative electrospray ionization. *Rapid Commun. Mass Spectrom.* **21**, 1721-1728.
Oyadomari, S., Koizumi, A., Takeda, K., Gotoh, T., Akira, S., Araki, E. and Mori, M. (2002). Targeted disruption of the Chop gene delays endoplasmic reticulum stress-mediated diabetes. *J. Clin. Invest.* **109**, 525-532.
Ozcan, U., Cao, Q., Yilmaz, E., Lee, A. H., Iwakoshi, N. N., Ozdelen, E., Tuncman, G., Gorgun, C., Glimcher, L. H. and Hotamisligil, G. S. (2004). Endoplasmic reticulum stress links obesity, insulin action, and type 2 diabetes. *Science* **306**, 457-461.
Palavalli, L. H., Brendza, K. M., Haakenson, W., Cahoon, R. E., Mclaird, M., Hicks, L. M., Mccarter, J. P., Williams, D. J., Hresko, M. C. and Jez, J. M. (2006). Defining the role of phosphomethylethanolamine N-methyltransferase from Caenorhabditis elegans in phosphocholine biosynthesis by biochemical and kinetic analysis. *Biochemistry* **45**, 6056-6065.
Pattingre, S., Bauvy, C., Carpentier, S., Levade, T., Levine, B. and Codogno, P. (2009). Role of JNK1-dependent Bcl-2 phosphorylation in ceramide-induced macroautophagy. *J. Biol. Chem.* **284**, 2719-2728.
Promlek, T., Ishiwata-Kimata, Y., Shido, M., Sakuramoto, M., Kohno, K. and Kimata, Y. (2011). Membrane aberrancy and unfolded proteins activate the endoplasmic reticulum stress sensor Ire1 in different ways. *Mol. Biol. Cell* **22**, 3520-3532.
Puri, P., Baillie, R. A., Wiest, M. M., Mirshahi, F., Choudhury, J., Cheung, O., Sargeant, C., Contos, M. J. and Sanyal, A. J. (2007). A lipidomic analysis of nonalcoholic fatty liver disease. *Hepatology* **46**, 1081-1090.
Rinella, M. E. and Sanyal, A. J. (2015). NAFLD in 2014: genetics, diagnostics and therapeutic advances in NAFLD. *Nat. Rev. Gastroenterol. Hepatol.* **12**, 65-66.
Rual, J.F., Ceron, J., Koreth, J., Hao, T., Nicot, A.S, Hirozane-Kishikawa, T., Vandenhaute, J., Orkin, S. H., Hill, D. E., van den Heuvel, S. and Vidal, M. (2004). Toward improving Caenorhabditis elegans phenome mapping with an ORFeome-based RNAi library. *Genome Res.* **14**, 2162-2168.
Rubio, C., Pincus, D., Korennykh, A., Schuck, S., El-Samad, H. and Walter, P. (2011). Homeostatic adaptation to endoplasmic reticulum stress depends on Ire1 kinase activity. *J. Cell Biol.* **193**, 171-184.
Rutkowski, D. T., Arnold, S. M., Miller, C. N., Wu, J., Li, J., Gunnison, K. M., Mori, K., Sadighi Akha, A. A., Raden, D. and Kaufman, R. J. (2006). Adaptation to ER stress is mediated by differential stabilities of pro-survival and pro-apoptotic mRNAs and proteins. *PLoS Biol.* **4**, e374.
Schroder, M. and Kaufman, R. J. (2005). ER stress and the unfolded protein response. *Mutat. Res.* **569**, 29-63.
Senft, D. and Ronai, Z. A. (2015). UPR, autophagy, and mitochondria crosstalk underlies the ER stress response. *Trends Biochem. Sci.* **40**, 141-148.
Shen, X., Zhang, K. and Kaufman, R. J. (2004). The unfolded protein response–a stress signaling pathway of the endoplasmic reticulum. *J. Chem. Neuroanat.* **28**, 79-92.
Shen, X., Ellis, R. E., Sakaki, K. and Kaufman, R. J. (2005). Genetic interactions due to constitutive and inducible gene regulation mediated by the unfolded protein response in C. elegans. *PLoS Genet.* **1**, e37.
Silvestrini, M. J., Johnson, J. R., Kumar, A. V., Thakurta, T. G., Blais, K., Neill, Z. A., Marion, S. W., St Amand, V., Reenan, R. A. and Lapierre, L. R. (2018). Nuclear export inhibition enhances HLH-30/TFEB activity, autophagy, and lifespan. *Cell Rep.* **23**, 1915-1921.
Singh, R., Kaushik, S., Wang, Y., Xiang, Y., Novak, I., Komatsu, M., Tanaka, K., Cuervo, A. M. and Czaja, M. J. (2009). Autophagy regulates lipid metabolism. *Nature* **458**, 1131-1135.
Smulan, L. J., Ding, W., Freinkman, E., Gujja, S., Edwards, Y. J. K. and Walker, A. K. (2016). Cholesterol-independent SREBP-1 maturation is linked to ARF1 inactivation. *Cell Rep* **16**, 9-18.
So, J.-S., Hur, K. Y., Tarrio, M., Ruda, V., Frank-Kamenetsky, M., Fitzgerald, K., Koteliansky, V., Lichtman, A. H., Iwawaki, T., Glimcher, L. H. et al. (2012). Silencing of lipid metabolism genes through IRE1alpha-mediated mRNA decay lowers plasma lipids in mice. *Cell Metab.* **16**, 487-499.
Sriburi, R., Jackowski, S., Mori, K. and Brewer, J. W. (2004). XBP1: a link between the unfolded protein response, lipid biosynthesis, and biogenesis of the endoplasmic reticulum. *J. Cell Biol.* **167**, 35-41.
Stiernagle, T. (2006). Maintenance of C. elegans. *WormBook* 1-11.
Supek, F., Bošnjak, M., Škunca, N. and Šmuc, T. (2011). REVIGO summarizes and visualizes long lists of gene ontology terms. *PLoS ONE* **6**, e21800.
Takacs-Vellai, K., Vellai, T., Puoti, A., Passannante, M., Wicky, C., Streit, A., Kovacs, A. L. and Müller, F. (2005). Inactivation of the autophagy gene bec-1 triggers apoptotic cell death in C. elegans. *Curr. Biol.* **15**, 1513-1517.
Talloczy, Z., Jiang, W., Virgin, H. W. T., Leib, D. A., Scheuner, D., Kaufman, R. J., Eskelinen, E.-L. and Levine, B. (2002). Regulation of starvation- and virus-induced autophagy by the eIF2alpha kinase signaling pathway. *Proc. Natl. Acad. Sci. USA* **99**, 190-195.

Tam, A. B., Roberts, L. S., Chandra, V., Rivera, I. G., Nomura, D. K., Forbes, D. J. and Niwa, M. (2018). The UPR activator ATF6 responds to proteotoxic and lipotoxic stress by distinct mechanisms. *Dev. Cell* **46**, 327-343 e7.

Thibault, G., Ismail, N. and Ng, D. T. W. (2011). The unfolded protein response supports cellular robustness as a broad-spectrum compensatory pathway. *Proc. Natl. Acad. Sci. USA* **108**, 20597-20602.

Thibault, G., Shui, G., Kim, W., McAlister, G. C., Ismail, N., Gygi, S. P., Wenk, M. R. and Ng, D. T. (2012). The membrane stress response buffers lethal effects of lipid disequilibrium by reprogramming the protein homeostasis network. *Mol. Cell* **48**, 16-27.

Tian, Y., Li, Z., Hu, W., Ren, H., Tian, E., Zhao, Y., Lu, Q., Huang, X., Yang, P., Li, X. et al. (2010). C. elegans screen identifies autophagy genes specific to multicellular organisms. *Cell* **141**, 1042-1055.

Timmons, L. and Fire, A. (1998). Specific interference by ingested dsRNA. *Nature* **395**, 854.

Tiniakos, D. G., Vos, M. B. and Brunt, E. M. (2010). Nonalcoholic fatty liver disease: pathology and pathogenesis. *Annu. Rev. Pathol.* **5**, 145-171.

Travers, K. J., Patil, C. K., Wodicka, L., Lockhart, D. J., Weissman, J. S. and Walter, P. (2000). Functional and genomic analyses reveal an essential coordination between the unfolded protein response and ER-associated degradation. *Cell* **101**, 249-258.

Urano, F., Calfon, M., Yoneda, T., Yun, C., Kiraly, M., Clark, S. G. and Ron, D. (2002). A survival pathway for Caenorhabditis elegans with a blocked unfolded protein response. *J. Cell Biol.* **158**, 639-646.

Vidal, R. L., Figueroa, A., Court, F. A., Thielen, P., Molina, C., Wirth, C., Caballero, B., Kiffin, R., Segura-Aguilar, J., Cuervo, A. M. et al. (2012). Targeting the UPR transcription factor XBP1 protects against Huntington's disease through the regulation of FoxO1 and autophagy. *Hum. Mol. Genet.* **21**, 2245-2262.

Volmer, R. and Ron, D. (2015). Lipid-dependent regulation of the unfolded protein response. *Curr. Opin. Cell Biol.* **33**, 67-73.

Volmer, R., Van Der Ploeg, K. and Ron, D. (2013). Membrane lipid saturation activates endoplasmic reticulum unfolded protein response transducers through their transmembrane domains. *Proc. Natl. Acad. Sci. USA* **110**, 4628-4633.

Walker, A. K., Jacobs, R. L., Watts, J. L., Rottiers, V., Jiang, K., Finnegan, D. M., Shioda, T., Hansen, M., Yang, F., Niebergall, L. J. et al. (2011). A conserved SREBP-1/phosphatidylcholine feedback circuit regulates lipogenesis in metazoans. *Cell* **147**, 840-852.

Walkey, C. J., Yu, L., Agellon, L. B. and Vance, D. E. (1998). Biochemical and evolutionary significance of phospholipid methylation. *J. Biol. Chem.* **273**, 27043-27046.

Walter, P. and Ron, D. (2011). The unfolded protein response: from stress pathway to homeostatic regulation. *Science* **334**, 1081-1086.

Wang, S., Chen, Z., Lam, V., Han, J., Hassler, J., Finck, B. N., Davidson, N. O. and Kaufman, R. J. (2012). IRE1alpha-XBP1s induces PDI expression to increase MTP activity for hepatic VLDL assembly and lipid homeostasis. *Cell Metab.* **16**, 473-486.

Wang, C., Saar, V., Leung, K. L., Chen, L. and Wong, G. (2018). Human amyloid beta peptide and tau co-expression impairs behavior and causes specific gene expression changes in Caenorhabditis elegans. *Neurobiol. Dis.* **109**, 88-101.

Wei, Y., Pattingre, S., Sinha, S., Bassik, M. and Levine, B. (2008a). JNK1-mediated phosphorylation of Bcl-2 regulates starvation-induced autophagy. *Mol. Cell* **30**, 678-688.

Wei, Y., Sinha, S. and Levine, B. (2008b). Dual role of JNK1-mediated phosphorylation of Bcl-2 in autophagy and apoptosis regulation. *Autophagy* **4**, 949-951.

Willy, J. A., Young, S. K., Stevens, J. L., Masuoka, H. C. and Wek, R. C. (2015). CHOP links endoplasmic reticulum stress to NF-kappaB activation in the pathogenesis of nonalcoholic steatohepatitis. *Mol. Biol. Cell* **26**, 2190-2204.

Wu, H., Ng, B. S. and Thibault, G. (2014). Endoplasmic reticulum stress response in yeast and humans. *Biosci. Rep.* **34**.

Yamamoto, K., Takahara, K., Oyadomari, S., Okada, T., Sato, T., Harada, A. and Mori, K. (2010). Induction of liver steatosis and lipid droplet formation in ATF6alpha-knockout mice burdened with pharmacological endoplasmic reticulum stress. *Mol. Biol. Cell* **21**, 2975-2986.

Younce, C. and Kolattukudy, P. (2012). MCP-1 induced protein promotes adipogenesis via oxidative stress, endoplasmic reticulum stress and autophagy. *Cell. Physiol. Biochem.* **30**, 307-320.

Zhang, Y., Yan, L., Zhou, Z., Yang, P., Tian, E., Zhang, K., Zhao, Y., Li, Z., Song, B., Han, J. et al. (2009). SEPA-1 mediates the specific recognition and degradation of P granule components by autophagy in C. elegans. *Cell* **136**, 308-321.

Zhao, Y., Li, X., Cai, M. Y., Ma, K., Yang, J., Zhou, J., Fu, W., Wei, F. Z., Wang, L., Xie, D. et al. (2013). XBP-1u suppresses autophagy by promoting the degradation of FoxO1 in cancer cells. *Cell Res.* **23**, 491-507.

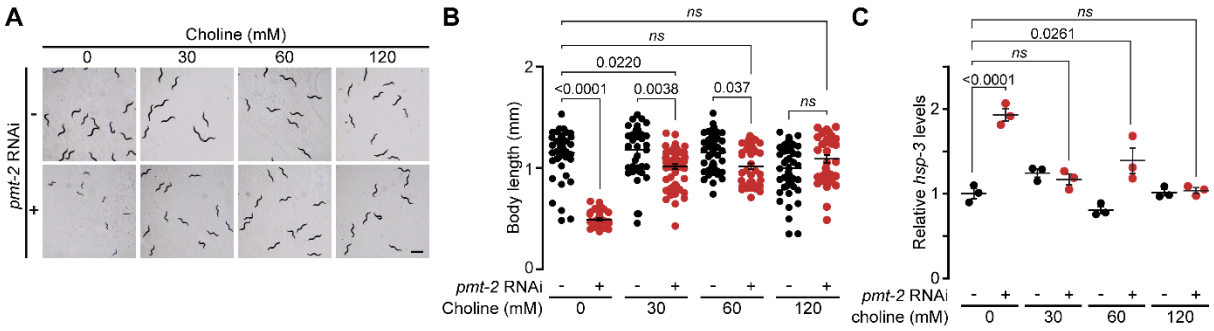

Figure S1, Refers to **Figure 1**. **Choline supplementation restores developmental defects in *pmt-2(RNAi)* animals.**
(A) Representative choline rescue assay of *pmt-2(RNAi)* developmental defect. L1 worms were grown on *pmt-2* RNAi or empty vector on plates supplemented with 0, 30, 60, or 120 mM choline, and images were taken after 48 h. Scale bar, 100 µm. (B) Body length quantification of worms from **A**. WT, 0 mM choline, n=47(-), n=32(+); 30 mM choline, n=39(-), n=58(+); 60 mM choline, n=48(-), n=43(+); 120 mM choline, n=54(-), n=38(+). (C) qPCR of *hsp-3* expression level in WT worms treated as in **A**. Data shown is the mean ± s.e.m. of at least three independent experiments. Statistical analysis was subjected to one-way ANOVA followed by Tukey's multiple comparisons adjustment. ns, non-significant.

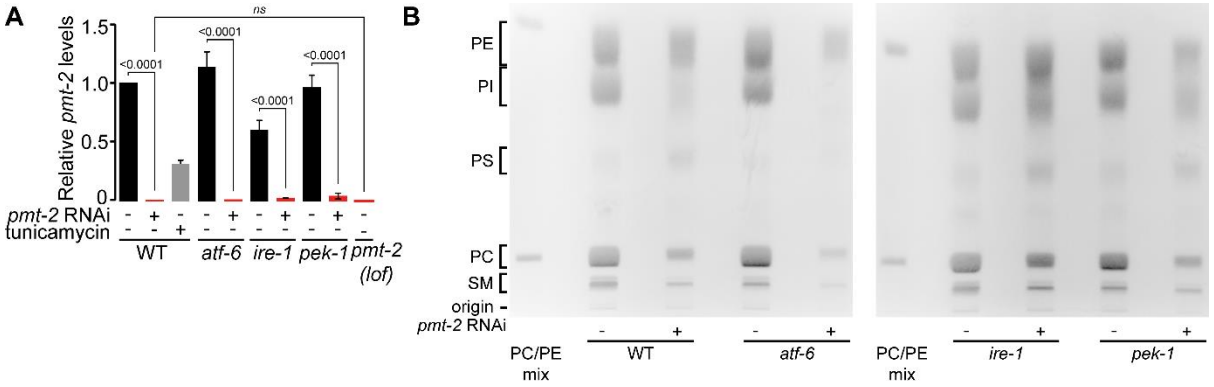

Figure S2, Refers to **Figure 2A-B**. **Inactivation of *pmt-2* decreased PC content in worms.**
(A) qPCR of *pmt-2* expression after *pmt-2* RNAi treatment in WT, *atf-6(lof)*, *ire-1(lof),* and *pek-1(lof)* worms. *pmt-2(lof)* worms were used as a control. *pmt-2* RNAi treatment efficiently silenced expression of *pmt-2* across all the strains tested. (B) Representative separation of PE, MMPE, DMPE, and PC from total lipid extract using thin-layer chromatography (TLC). Comparison of phospholipid levels in WT, *atf-6(lof)*, *ire-1(lof)* and *pek-1(lof)* animals treated with *pmt-2* RNAi. POPE (1-palmitoyl-2-oleoyl-sn-glycero-3-phosphoethanolamine; 16:0-18:1n9 PE) and DOPC (1,2-dioleoyl-sn-glycero-3-phosphocholine; 18:1n9 PC) were used as markers. Data shown is the mean ± s.e.m. of at least three independent experiments. Statistical analysis was subjected to one-way ANOVA followed by Tukey's multiple comparisons adjustment. ns, non-significant.

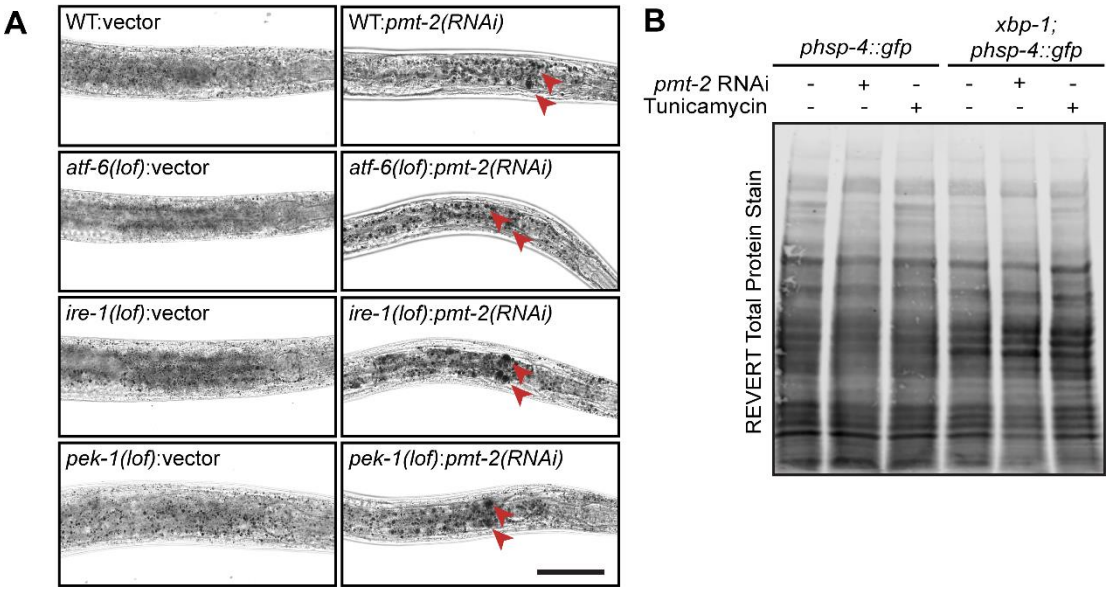

Figure S3, Refers to **Figure 2C,F**. **Lipid perturbation induces lipid droplets accumulation and activates the UPR.**
(A) Representative images of lipid droplet visualised using Sudan Black B staining of WT, *atf-6(lof)*, *ire-1(lof)* and *pek-1(lof)* animals treated with *pmt-2* RNAi. Brightfield images of stained worms are shown using 63X objective lens. Red arrowhead highlights large LDs. Scale bar, 100 µm. (B) Total protein stain verified equal loading and served as normalization control for the immunoblot.

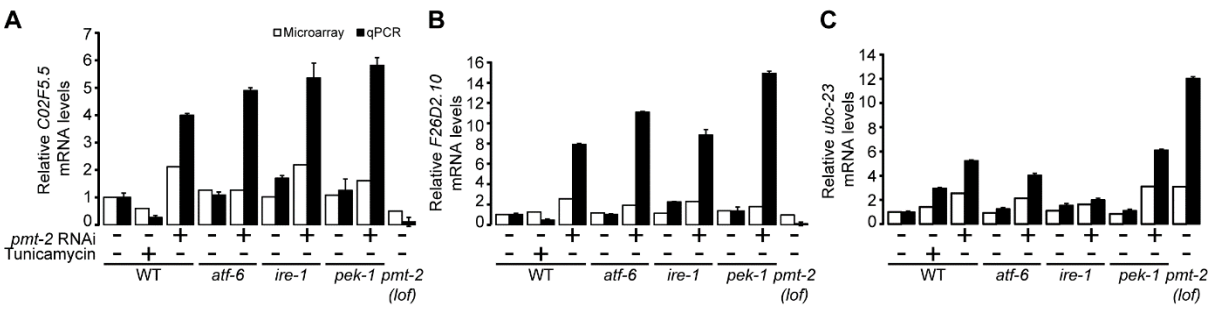

Figure S4, Refers to **Figure 3**. **Validation of DNA microarray analysis using quantitative real-time PCR.**
(A-C) Comparison of *C02F5.5* (A), *F26D2.10* (B), and *ubc-23* (C) gene expression in WT, *atf-6(lof)*, *ire-1(lof)* and *pek-1(lof)* animals treated with *pmt-2* RNAi by DNA microarray (white bars) and qPCR (black bars). *C02F5.5* and *F26D2.10*, are both uncharacterized genes; *ubc-23*, a member of the BCL-2 family. The figure represents technical triplicates.

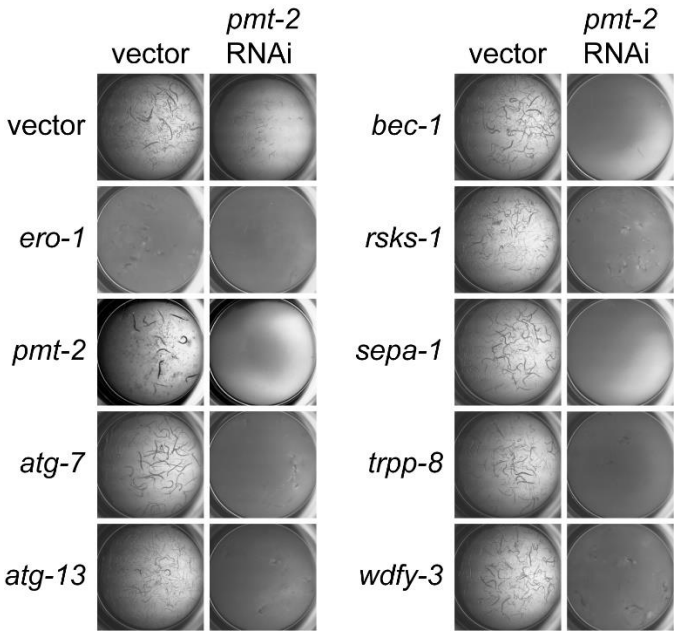

Figure S5, Refers to Figure 5. **Autophagy is essential during lipid perturbation.** WT worms were treated with vector or *pmt-2* RNAi for 36 h and subsequently subjected to RNAi in liquid media in a 96-well plate for 5 days. The worms were scored based on their developmental defects as described in Fig. 5A. *ero-1* RNAi was included as a positive control.

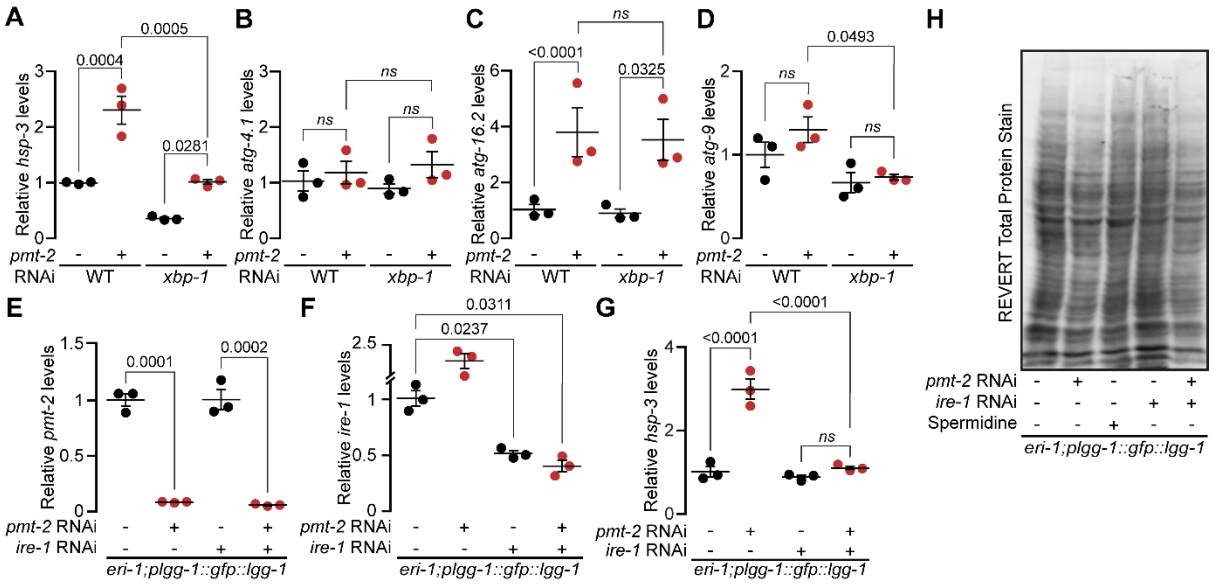

Figure S6, Refers to Figure 5. **Autophagy is partially dependent on XBP-1**. qPCR comparing expression of *hsp-3* (A), *atg-4.1* (B), *atg-16.2* (C), *atg-9* (D) in WT and *xbp-1(lof)* mutants treated with *pmt-2* RNAi. qPCR comparing expression of *pmt-2* (E), *ire-1* (F), *hsp-3* (G) in *eri-1;plgg-1::gfp::lgg-1* worms treated with *pmt-2, ire-1*, and *ire-1:pmt-2* RNAis; technical triplicates. (H) Total protein stain verified equal loading and served as normalization control for the immunoblot. Data shown is the mean ± s.e.m. of at least three independent experiments. Statistical analysis was subjected to one-way ANOVA followed by Tukey's multiple comparisons adjustment. ns, non-significant.

Table S1. Oligonucleotide primers used in the study.

Gene	Sequence (5' to 3')	Assay
act-1	AGGACTGGGTGCTCTTCTGG GAGCACGGTATCGTCACCAA	qPCR
atg-4.1	AGGAAGATGGAATCGAGGCAA TGCAACCCCATCCTTGATCC	qPCR
atg-9	ATGGAATCGTTCTTCTCACTG GCAGGAGGTATTGTATCTTCTC	qPCR
atg-16.2	ATGTGCTGGCTGGATCTTCG GAGCCGAATCTGATCTCGCAG	qPCR
atg-18	CCGAAGTCAGACACTAGTCGAG TCGGAACCGATTGGTTGCTTG	qPCR
bec-1	AAGCTCTGACTGGACATTCTCG GCGTCAGAGCAATCATTACAAAC	qPCR
atg-18	CCGAAGTCAGACACTAGTCGAG TCGGAACCGATTGGTTGCTTG	qPCR
C02F5.5	CATCTTTTGAGCTTATGATGGTGCT AAGCACCAAGGAACACGAGAT	qPCR
epg-4	CCAATTCCTCTTATCACACCA GTCGAAGAAGTAATCGAAACAG	qPCR
F26D2.10	CTCTTGTGGCAGCTCATGGT CGTGGATCAAAAACAGCGGC	qPCR
hsp-3	AGAAGGAGACCAAGTATGGAACC TGATACGGTTTCCTTGGTCGTT	qPCR
hsp-4	CATCTCGTGGAATCAACCCT TGACGTCAAGAAGGACAACA	qPCR
lgg-1	TCGTGATGGTCCTGGTAGAGT ACGCATCCAACTTCGTCCA	qPCR
ire-1	ACAATGGCTAGTCAGCGAGG CAATCCAGCCATCGGTTCCT	qPCR
pmt-2	AGAACGTGGTCATTTGGAGCAG TTCGCGTTGGGTAAACTTCGAC	qPCR

Table S2, Refers to **Figure 3A**. **List of upregulated and downregulated genes in *pmt-2(RNAi)* and WT treated with tunicamycin compared to WT animals.** Excel Spreadsheet

Click here to Download Table S2

Table S3, Refers to **Figure 3B**. **List of upregulated genes from the four-way Venn diagram.** Excel Spreadsheet

Click here to Download Table S3

Table S4, Refers to **Figure 3C**. **Hierarchical clustering gene list.** Excel Spreadsheet

Click here to Download Table S4

Table S5, Refers to **Figure 4**. **Predominant GO terms of each cluster.** Excel Spreadsheet

Click here to Download Table S5

Table S6, Refers to **Figure 5**. **Phenotype from RNAi screen of autophagy genes.** Excel Spreadsheet

Click here to Download Table S6